Dynamic reconfiguration of functional brain networks during working memory training

Karolina Finc[1*], Kamil Bonna[1,2], Xiaosong He[3], David M. Lydon-Staley[3], Simone Kühn[4,5], Włodzisław Duch[1,2], and Danielle S. Bassett[3,7,8,9,10]

[1] *Centre for Modern Interdisciplinary Technologies, Nicolaus Copernicus University in Toruń, Poland*
[2] *Institute of Physics, Faculty of Physics, Astronomy and Informatics, Nicolaus Copernicus University in Toruń, Poland*
[3] *Department of Bioengineering, School of Engineering and Applied Science, University of Pennsylvania, Philadelphia, PA, 19104 USA*
[4] *Center for Lifespan Psychology, Max Planck Institute for Human Development, Berlin, Germany*
[5] *University Medical Center Hamburg - Eppendorf, Hamburg, Germany*
[7] *Department of Electrical & Systems Engineering, School of Engineering and Applied Science, University of Pennsylvania, Philadelphia, PA, 19104 USA*
[8] *Department of Neurology, Perelman School of Medicine, University of Pennsylvania, Philadelphia, PA, 19104 USA*
[9] *Department of Physics & Astronomy, School of Arts and Sciences, University of Pennsylvania, Philadelphia, PA, 19104 USA*
[10] *Department of Psychiatry, Perelman School of Medicine, University of Pennsylvania, Philadelphia, PA, 19104 USA*
[*] *finc@umk.pl*

June 27, 2019

Abstract

The functional network of the human brain continually adapts to changing environmental demands. Such adaptation spans multiple time scales, from seconds during task performance to days and weeks during motor or cognitive training. Yet the precise consequence of behavioral automation for functional network architecture, particularly in the context of complex tasks, remains far from understood. Here we investigated the neural reflections of behavioral adaptation as human participants mastered a dual n-back task over 6 weeks of training. In four fMRI scans equally spanning the training period, we assessed the level of brain network modularity, a common substrate for adaptation in biological systems. Specifically, we investigated both static and dynamic modularity to probe the segregation between task-relevant fronto-parietal and default mode systems, and to assess their time-evolving recruitment and integration. We found that whole-brain modularity was higher during the resting state than during the dual n-back task, and increased as demands heightened from the 1-back to the 2-back condition. Modularity also steadily increased in response to training for both task conditions. In an explicitly dynamic analysis, we found that the recruitment of both the default mode and fronto-parietal systems during the dual n-back task was modulated by training. Moreover, the change in default mode recruitment from the first scanning session to the last was positively correlated with behavioral improvement after training. Reliably across static and dynamic network analyses, our findings suggest that the automation of a cognitively demanding task may result in more segregated network organization.

INTRODUCTION

The brain constantly adjusts its architecture to meet the demands of the ever-changing environment. Such neural adaptation spans multiple time scales, being observed over seconds to minutes during task performance (Braun et al., 2015; Vatansever et al., 2015; Cohen and D'Esposito, 2016; Shine et al., 2016; Finc et al., 2017), over days to weeks during learning (Bassett et al., 2013, 2015; Mohr et al., 2016), and over years during development (Betzel et al., 2014). Like many other complex biological systems, the adaptability of the brain is supported by its modular structure (Friston, 2009; Sporns, 2013). Intuitively, modularity allows for dynamic switching between states of segregated and integrated information processing, whose balance is constantly adjusted to meet the requirements of our cognitive faculties (Bullmore and Sporns, 2012; Shine and Poldrack, 2018). Understanding the patterns of these adjustments and determining the rules that explicate their relation to human behavior is one of the most important challenges for cognitive neuroscience.

It is hypothesized that simple, highly automated sensorimotor tasks can be maintained by a highly segregated brain organization, while more complex and cognitively demanding tasks require integration between multiple subnetworks (Dehaene et al., 1998). Indeed, switching from a segregated to a more costly integrated network architecture is consistently reported as human participants transition to challenging tasks with heavy cognitive load (Braun et al., 2015; Kitzbichler et al., 2011; Vatansever et al., 2015; Shine et al., 2016; Cohen and D'Esposito, 2016; Finc et al., 2017); in contrast, network organization during simple motor tasks remains highly segregated (Cohen and D'Esposito, 2016; Shine et al., 2016). Whether shifts towards network integration depend on the level of task complexity or on the level of task automation remains to be delineated (Shine and Poldrack, 2018). Is it possible that a complex, but fully automated task, can be performed without the need for costly network integration?

Longitudinal studies, during which participants are scanned multiple times while mastering a specific task, can shed light on patterns of network adaptation related to learning and task automation (Shine and Poldrack, 2018). For example, Bassett et al. (2015) showed that training on a visuomotor task over the course of 6 weeks leads to increased autonomy between task-relevant subnetworks in motor and visual cortices. In another study, Mohr et al. (2016) found increased segregation of the default mode system after short-term visuomotor training. Collectively, these findings suggest that an increase in network segregation and a decrease in integration may constitute a natural consequence of task automation. However, these results refer to the training of simple motor tasks, which do not require extensive network integration, in contrast to complex tasks involving higher order cognitive functions such as cognitive control (Shine and Poldrack, 2018). The consequence of complex cognitive task automation on the balance between network segregation and network integration remains unknown.

In the present study, we investigated whether mastering a demanding working memory task affects the balance between network segregation and integration during task performance. Does effortless performance of the demanding cognitive task lead to the same increase in network segregation that is characteristic of simple motor tasks (Cohen and D'Esposito, 2016; Mohr et al., 2016)? Is the breakdown of network segregation during the changing demands of the cognitive task still necessary when the cognitive task is automated? Finally, do we observe stronger separation of subnetworks relevant to cognitive control when tracking dynamical brain network reorganization throughout the course of training? To address these questions, participants underwent four functional magnetic resonance imaging (fMRI) scans while performing an adaptive dual n-back task taxing working memory over a 6-week training period. To ensure that participants achieved mastery in the task due to training, and not simply due to repeated exposure to the task, we compared their performance to an active control group. We examined network reconfiguration using static functional network measures to distinguish distinct task conditions, and using dynamic network measures to study fluctuations of network topology across short task blocks.

First, we investigated global changes in network segregation (modularity) across different task conditions as compared to rest. In line with the aforementioned research, we expected modularity to decrease during dual n-back task performance compared to rest, and also to decrease as the demands of the n-back task increased. We also hypothesized that over the course of training network segregation during the n-back task would increase, and the extent of demand-related modularity change would decrease. In the systems relevant to working memory performance – the frontoparietal and the default mode systems (Cocchi et al., 2013) – we expected an increase in autonomy throughout the course of training. To verify this hypothesis, we utilized previously developed dynamic network methods (Bassett et al., 2015) to assess the recruitment and integration of the default mode and fronto-parietal systems. Finally, we expected that changes in network architecture would correspond to the level of task automation and training progress.

RESULTS

Behavioral changes during training

Behavioral improvement in the task can either occur as a result of training or occur in response to repeated exposure to a task across multiple scanning sessions. To distinguish the effect of intensive working memory practice and task automation from the effect of repeated exposure, we employed an active control group. When participants from the experimental group underwent the challenging, adaptive, dual n-back working memory training, participants from the control group performed a single, non-adaptive, 1-back working memory task (Fig. 1).

The dual n-back task (1-back and 2-back conditions) was performed in the scanner on the first day of the experiment (Naive), after two weeks of training (Early), after four weeks of training (Middle), and after six weeks of training (Late). We measured participant performance as a penalized reaction time (pRT), which incorporates a measure of accuracy (see **Methods**). Better cognitive performance is characterized by lower values of pRT. We expected that participants from the experimental group would exhibit a substantial decrease of pRT during training, particularly for the 2-back condition in comparison to the 1-back condition,

the latter being easy to master even without extensive training.

Using multilevel modelling (see **Methods**), we found that participants had significantly different pRT depending on the training stage (Naive, Early, Middle, Late), condition (1-back vs. 2-back), and group (Experimental vs. Control). Specifically, we found a significant session × condition × group interaction ($\chi^2(3) = 22.83$, $p = 0.00004$; Fig. 2). The greatest improvement was observed in the experimental group when comparing 'Naive' to 'Late' training phases during the 2-back condition (mean 43.4% pRT improvement; Bonferroni-corrected, $t(22) = 10.39$, $p < 0.0001$). For comparison, the control group exhibited only a 10.7% decrease of pRT during the 2-back condition (Bonferroni-corrected, $t(22) = 3.54$, $p = 0.002$). The decrease in pRT was significantly larger for the experimental group than for the control group (Bonferroni-corrected, $t(43.576) = 5.34$, $p < 0.0001$; Fig. 2d). In the 1-back condition, the experimental group displayed a 12.5% reduction in pRT (Bonferroni-corrected, $t(22) = 3.86$, $p = 0.0008$); no improvement was found in the control group ($t(22) = 1.90$, $p = 0.07$) (see Fig. 2c). The change in pRT during the 1-back condition did not differ between the two groups ($t(44) = 1.39$, $p = 0.17$). Interestingly, in experimental group we observed no significant difference in performance between the 1-back condition and the 2-back condition after training (Bonferroni-corrected, $t(22) = 1.85$, $p = 0.08$). This finding suggests that the 2-back condition, which was much more effortful before training ('Naive' phase), was performed effortlessly after training, at the same level as the 1-back task.

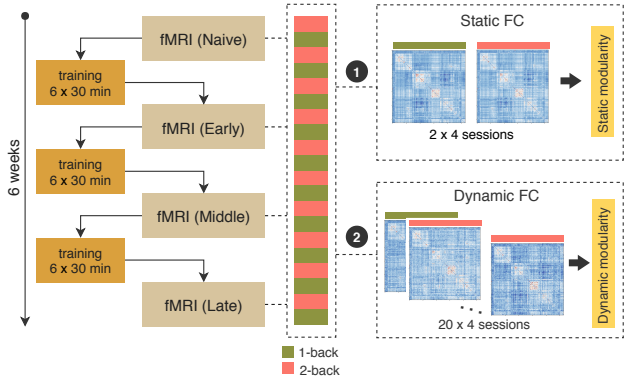

Figure 1: **Study design.** *(Left)* The dual n-back working memory task was performed in the scanner on the first day of the experiment (Naive), after 2 weeks of training (Early), after 4 weeks of training (Middle), and after 6 weeks of training (Late). *(Right)* We investigated **(1)** changes in static modularity across task conditions (1-back versus 2-back) and **(2)** dynamic fluctuations in network community structure from block to block.

In sum, the results demonstrate that the experimental group gradually improved in behavioral performance measured during the fMRI scanning sessions, and that this improvement was significantly greater than the corresponding effect in the control group. We also replicated these findings using an alternative measure of behavior, d-prime, which has historically proven useful in probing human performance on the n-back task (see Fig. S3).

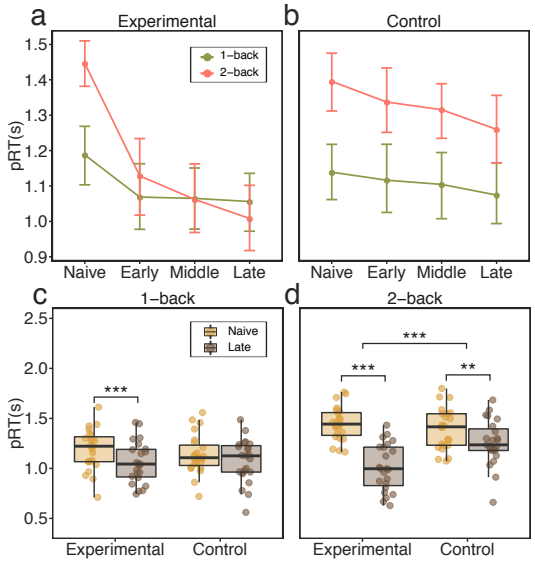

Figure 2: **Behavioral performance modulated by training.** **(a, b)** Line plots representing mean behavioral performance measured as penalized reaction time (pRT), calculated for all training phases (Naive, Early, Middle, Late), dual n-back conditions (1-back and 2-back), and groups (**(a)** experimental and **(b)** control). We found a significant interaction effect between session, condition, and group ($\chi^2(3) = 22.83$, $p = 0.00004$). After training, the experimental group exhibited no difference in behavioral performance between the 1-back and 2-back conditions. **(c)** No significant difference between groups was found for pRT reduction (from Naive to Late sessions) during the 1-back task condition. **(d)** The experimental group showed a significant reduction in pRT compared to the control group during the challenging 2-back condition. Error bars represent 95% confidence intervals. *** $p < 0.001$ Bonferroni corrected; ** $p < 0.01$ Bonferroni corrected.

Whole-brain network modularity changes

To establish whether complex working memory task training leads to increased network segregation at the whole-brain level, we investigated network modularity during different sessions and load conditions. Here, we employed a common community detection algorithm known as modularity maximization (Newman and Girvan, 2004), which we implemented using a Louvain-like locally greedy algorithm. The modularity quality function to be optimized encodes the extent to which the network can be divided into non-overlapping *communities*. Intuitively, a community is a group of densely interconnected nodes with sparse connections to the rest of the network (Newman and Girvan, 2004). Modularity is a relatively simple measure of segregation, with high values indicating greater segregation of the brain into non-overlapping communities and low values indicating lesser segregation. Because modularity depends

upon the network's total connectivity strength, we normalized each modularity score by dividing it by the mean of the corresponding null distribution calculated on a set of randomly rewired versions of the original networks (Maslov and Sneppen, 2002) (see **Methods** for details).

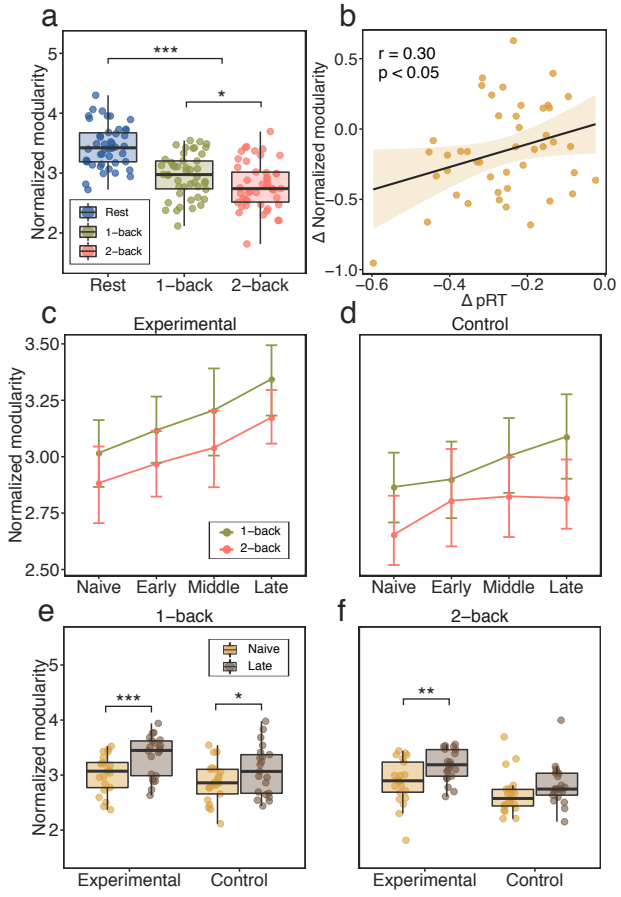

Figure 3: **Modularity differences across task, sessions, and groups.** (**a**) Modularity differences between resting and dual n-back task conditions. (**b**) Correlation between change (from 2-back to 1-back) of the normalized modularity and the change (from 2-back to 1-back) of behavioral performance as measured by a penalized reaction time (pRT). (**c, d**) Line plots representing the mean values of modularity for each scanning session (Naive, Late, Middle, Late) and condition, separately for (**c**) the experimental group and (**d**) the control group. (**e, f**) Modularity changes from 'Naive' to 'Late' sessions for the 1-back condition and the 2-back condition. Error bars represent 95% confidence intervals. *** $p < 0.001$ Bonferroni corrected; ** $p < 0.01$ Bonferroni corrected, * $p < 0.05$ uncorrected.

Functional network modularity may vary depending on the difficulty of the task. Several studies have reported a reduction in modular structure during demanding n-back conditions (Kitzbichler et al., 2011; Vatansever et al., 2015; Finc et al., 2017; Cohen and D'Esposito, 2016). Here, we first investigated the differences between the high-demand 2-back condition and the low-demand 1-back condition as compared to a baseline resting state scan acquired during the first session ('Naive') for all subjects. Using multilevel modeling we found a significant main effect of condition ($\chi^2(2) = 84.13$, $p < 0.00001$). Planned contrast analysis revealed that network modularity during the dual n-back task was lower than network modularity during the resting state (β = -0.20, $t(88)$ = -11.37, $p <$ 0.00001). Furthermore, modularity was significantly reduced during the 2-back condition relative to the 1-back condition (β = -0.08, $t(296)$ = -2.60, $p < 0.05$; Fig. 3a). We also found that the difference in modularity between the 2-back condition and the 1-back condition was significantly correlated with the difference in penalized reaction time between the two conditions (Pearson's r = 0.30, p = 0.04; Fig. 3b). The greater the decrease in modularity from 1-back to 2-back, the smaller the decline in performance, as measured by pRT, from 1-back to 2-back. This result is consistent with several prior studies which have reported an inverse association between modularity and behavioral performance (Vatansever et al., 2015; Shine et al., 2016; Finc et al., 2017). We note that the results reported here use a functional brain parcellation comprised of 264 regions of interests provided by Power et al. (2011); in robustness tests, we performed the same analyses using the Schaefer parcellation, and obtained similar results (see **Supplementary Materials**).

The modularity of functional brain network architecture decreases appreciably during challenging task conditions, but is the breakdown in modularity still present when the demanding task is mastered? To address this question, we tested whether modularity during the dual n-back task changed depending on the session, task condition, and group. Using a multilevel model (see **Methods**), we found a significant main effect of session ($\chi^2(2) = 19.40$, $p = 0.0002$). A planned contrast comparison showed that participants' whole-brain functional network modularity significantly increased from 'Naive' to 'Middle' sessions ($\beta = 0.15$, $t(114) = 2.61$, $p = 0.01$) and from 'Naive' to 'Late' sessions ($\beta = 0.24$, $t(114) = 4.05$, $p = 0.0001$). We observed no significant change in modularity between 'Naive' and 'Early' sessions (β = 0.08, $t(114)$ = 1.42, p = 0.15; Fig. 3cd). However, the experimental and control groups did not differ by session ($\chi^2(1) = 1.44$, $p = 0.69$), nor did we observe a significant session by condition interaction ($\chi^2(1)$ = 1.50, p = 0.68). To summarize, we showed that the modularity of the functional brain network generally increased during the training period. However, the degree to which modularity changed between load conditions remained stable. Groups did not differ significantly in the change of modularity. These results suggest that the functional brain network shifts towards a more segregated organization as a result of behavioral improvement after training and also after repeated exposure to the task. Although network modularity increased to a similar extent in both conditions, the demand-dependent change in modularity remained

stable. One could interpret these results as suggesting that a general increase in modularity reflects the fact that less expensive information processing is required within segregated brain subsystems after automation of the complex task.

To further explore the changes in modularity that might be specific to each group and condition, we performed additional analyses comparing modularity measured before and after training (Fig. 3ef). Specifically, we employed separate paired t-tests to investigate differences in modularity for each group and condition between 'Naive' and 'Late' sessions; because four separate tests were performed, we used a Bonferroni adjusted alpha level of 0.0125 per test to minimize the potential for false positives due to multiple comparisons. We found a significant increase of modularity in the experimental group in the 1-back condition (Bonferroni-corrected, $t(20)$ = -3.66, p = 0.001) and in the 2-back condition (Bonferroni-corrected, $t(20)$ = -3.33, p = 0.003). The increase in modularity observed in the control group was not significant after Bonferroni correction for either the 1-back condition (Bonferroni-corrected, $t(20)$ = -2.35, p = 0.03) or the 2-back condition ($t(20)$ = -1.88, p = 0.07). The change of modularity from 'Naive' to 'Late' sessions did not significantly differ between groups for the 1-back condition ($t(39.88)$ = -0.80, p = 0.42) or for the 2-back condition ($t(39.99)$ = -1.05, p = 0.30). Collectively, these results demonstrate that modularity increased for both 1-back and 2-back task conditions in the experimental group but only during the 1-back condition for the control group. The findings suggest that higher brain network segregation during the 2-back condition may be a consequence of the 6-week working memory training.

Behavioral gains resulting from working memory training differed across participants, suggesting the existence of individual differences in learning capabilities. Therefore, we also tested whether the increase of modularity observed during the 2-back condition in the experimental group was correlated with behavioral performance after training as measured by a decrease in pRT. However, we did not find a significant relationship between these two variables (Pearson's correlation coefficient r = 0.03, p = 0.73). This finding suggests that the change of modularity is a general consequence of training and may not reflect individual differences in behavioral improvement.

Our results confirmed the existence of a decrease in modularity during increased cognitive demands and an association between modularity and performance. However, changes in modularity during training were not different across conditions or experimental groups. A significant increase in modularity from 'Naive' to 'Late' sessions was found for the 1-back and 2-back conditions for the experimental group, which suggests the enhancement of network segregation associated with task automation.

Dynamic reorganization of default mode and fronto-parietal systems

The modular architecture of functional brain networks is not static but instead can fluctuate appreciably over task blocks. Here, we used a dynamic network approach to answer the question of whether systems relevant to working memory – the fronto-parietal and the default mode – change in their fluctuating patterns of expression during training. Based on a previous study of motor sequence learning (Bassett et al., 2015), we expected that these two systems would become more autonomous over the 6 weeks of working memory training. To formally test our expectation, we investigated the dynamic reconfiguration of the network's modular structure as subjects switched between blocks of the dual n-back task. Pooling across conditions and sessions, we constructed a multilayer network model of the data in which each block corresponds to a unique layer, each region corresponds to a node, and each functional connection corresponds to an edge. We then employed a multilayer community detection algorithm that estimates each node's module assignment in each network layer (Mucha et al., 2010). The presence of fluctuations in community structure across task blocks is indicated by variable assignments of nodes to modules across layers. For each subject and session, we summarized these data in a module allegiance matrix $\mathbf{P}$, where each element P_{ij} represents a proportion of blocks for which node i and node j were assigned to the same module. From $\mathbf{P}$ we calculated the recruitment and integration of the default mode and fronto-parietal systems (Fig. 4a; see **Methods** for details). Recruitment is defined for each system separately, while integration is calculated for the pair of systems. Intuitively, high recruitment indicates that nodes of the system are consistently assigned to the same module across different layers. High integration indicates that pairs of nodes (where one region of the pair is located in one system and the other region of the pair is located in the other system) are frequently classified in the same module across layers. We used a multilevel model to test whether recruitment and integration differed between scanning sessions and experimental groups.

Using a multilevel model, we observed a significant session × group interaction effect when considering changes in the recruitment of the fronto-parietal system during training ($\chi^2(3)$ = 11.90, p = 0.0079)(Fig. 4d). The largest increase in fronto-parietal recruitment was observed in the experimental group when comparing 'Naive' to 'Late' training phases (9.3% ; $t(20)$ = -3.51, $p < 0.002$, Bonferroni-corrected; Fig. 4b). No significant changes from 'Naive' to 'Late' training phases were observed in the control group ($t(20)$ = -1.69, p = 0.11). Turning to an examination of the default

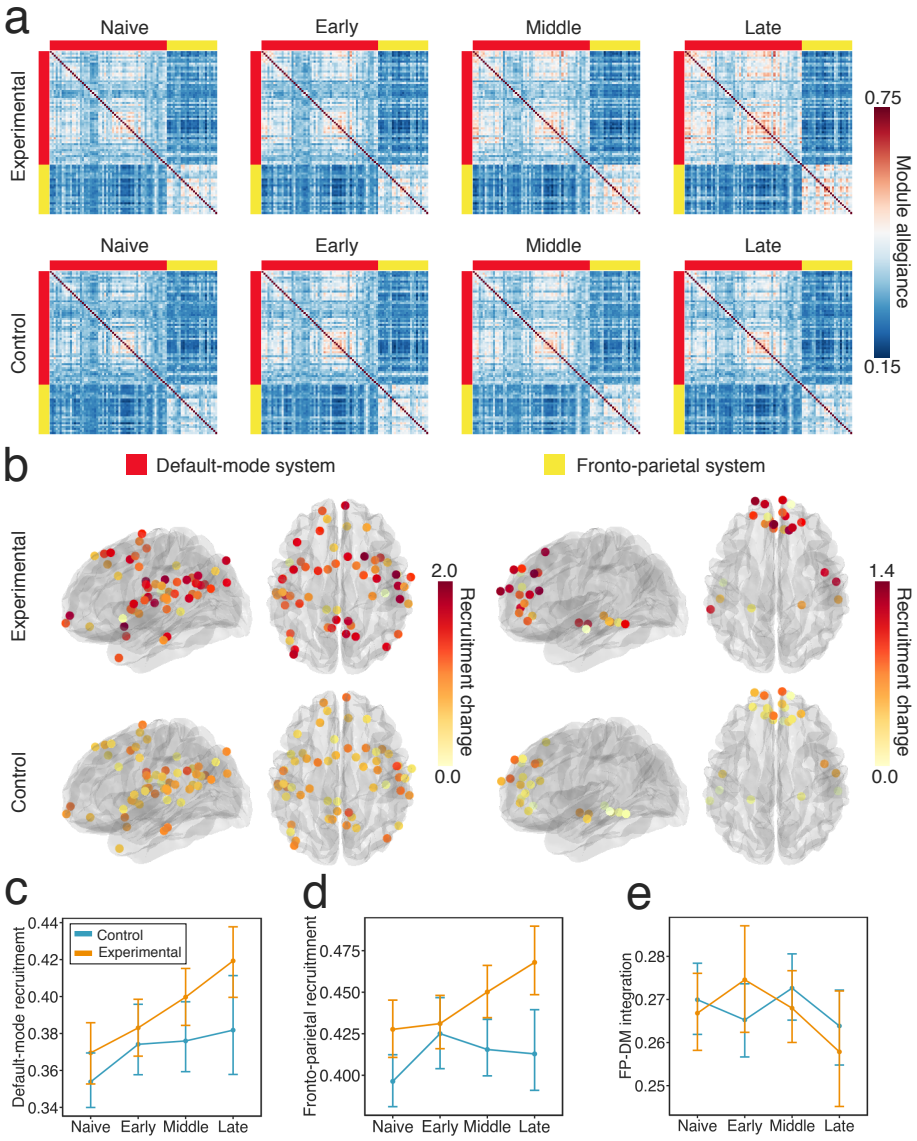

Figure 4: **Changes in module allegiance of the fronto-parietal (FP) and default-mode (DM) systems.** (**a**) Module allegiance matrices for default mode and fronto-parietal systems. Each ij-th element of the matrix represents the probability that node i and node j are assigned to the same module within a single layer of the multilayer network. (**b**) Recruitment changes from the 'Naive' to the 'Late' stages of training. Increased recruitment suggests better functional communication among the nodes within each system. (**c**) Both experimental and control groups exhibited increases in default mode recruitment between 'Naive' and 'Late' stages of training. (**d**) Only the experimental group exhibited increases in fronto-parietal recruitment across sessions. (**e**) In both groups, the integration between the fronto-parietal and default mode systems decreased from 'Naive' to 'Late' sessions.

mode, we found a significant main effect of session ($\chi^2(3) = 28.09$, $p < 0.0001$) and of group ($\chi^2(1) = 4.22$, $p = 0.04$) on system recruitment (Fig. 4c). However, the interaction effect between session and group was not significant ($\chi^2(3) = 4.52$, $p = 0.21$). Next we assessed differences between 'Naive' and 'Late' training phases for each group separately. The recruitment of the default mode system increased markedly in the experimental group (13.5%; $t(20) = -4.67$, $p = 0.0001$, Bonferroni-corrected), and less markedly in the control group (8.6%; $t(20) = -2.93$, $p = 0.008$, Bonferroni-corrected). We found a significant main effect of session on the integration between the fronto-parietal and default mode systems ($\chi^2(3) = 9.74$, $p < 0.02$) (Fig. 4e). The integration between these two systems decreased from 'Naive' to 'Late' sessions ($\beta = 0.08$, $t(123) = -2.18$, $p = 0.03$). The main effect of group was not significant ($\chi^2(1) = 0.03$, $p = 0.87$), and neither was the interaction between session and group ($\chi^2(3) = 6.60$, $p < 0.08$).

Next, we used multilevel modeling to investigate the relationship between across-session change in system recruitment or integration and across-session change in behavioral performance (see **Methods**). For both brain and behavioral variables, we measured the change from the first ('Naive') to the last ('Late') training sessions. We found a significant main effect of default mode recruitment change ($\chi^2(1) = 4.70$, $p < 0.05$; Fig. 5a), indicating that an increasing recruitment of the default mode was associated with improved behavioral performance, as operationalized by a change in pRT. Interestingly, the effect held irrespective of group membership, suggesting the relevance of this relationship to general task improvement. The groups did differ in the intercept ($\chi^2(1) = 12.65$, $p < 0.001$), with the experimental group displaying a greater predicted change in default mode recruitment for small changes in behavior, than was observed in the control group. In considering the fronto-parietal system, we did not find a main effect of the relationship between the change in recruitment and the change in behavior. We did, however, observe a main effect of group ($\chi^2(1) = 13.68$, $p < 0.001$; Fig. 5b), with a strong positive relationship between brain and behavior in the experimental group.

Dynamic fluctuations of default mode recruitment

We further examined changes in the default mode and fronto-parietal recruitment by calculating allegiance matrices for each task block. Does network recruitment vary between task conditions? To address this question, we took the module assignment vector of each network layer, and calculated the probability that a node was classified within the same community across all runs of the modularity optimization algorithm. We found a significant effect of condition ($\chi^2(3) = 83.97$, $p < 0.00001$; Fig. 6), such that the recruitment of the default mode fluctuated between task conditions and was significantly higher in the 1-back condition (M = 0.40) than in the 2-back condition (M = 0.36; $t(167) = -10.43$, $p < 0.00001$). However, the session × condition interaction was not significant ($\chi^2(3) = 2.82$, $p = 0.40$). When considering the fronto-parietal recruitment, we found no significant effect of condition ($\chi^2(3) = 2.65$, $p = 0.10$) or session × condition interaction ($\chi^2(3) = 4.95$, $p = 0.17$). Collectively, these results suggest that the default mode recruitment is not only modulated by working memory training, but also by the changing demands of the cognitive task.

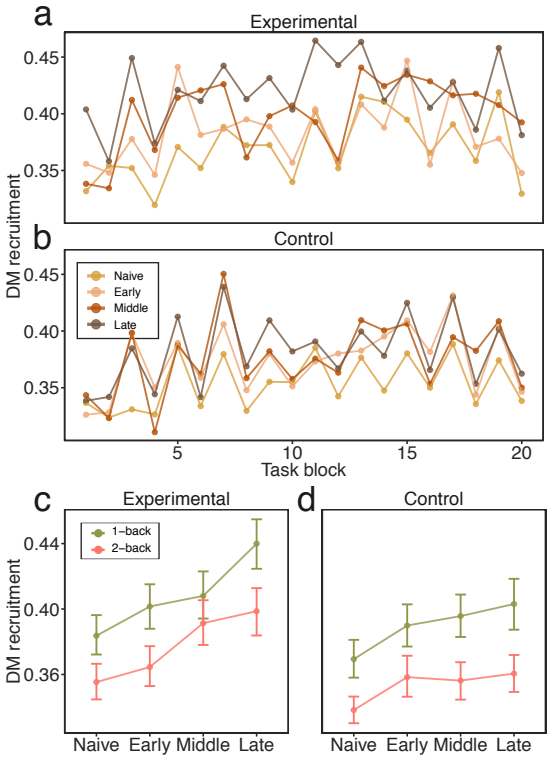

Figure 6: **Fluctuations in the recruitment of the default mode system across task blocks**. Across-block fluctuations in default mode recruitment in (**a**) the experimental group and (**b**) the control group. Differences between task conditions for (**c**) the experimental group and (**d**) the control group, across training stages.

Training related changes in other large-scale systems

We further investigated whether training-related changes were restricted to the default mode and fronto-parietal systems. To approach this question, we calculated the recruitment of each large-scale system and the integration between each pair of systems for the 'Naive' and 'Late' training phases (Fig. 7a). In the experimental group, we found that the recruitment of the default mode and fronto-parietal systems increased from the 'Naive' to the 'Late' training phase, as did the

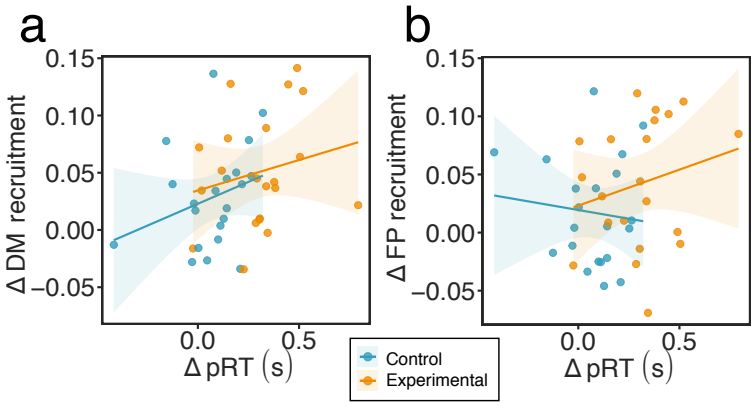

Figure 5: **Relationship between change in the recruitment of the default mode system and change in behavioral performance.** Change in system recruitment was calculated as a difference between the recruitment estimated in the 'Late' and 'Naive' scanning sessions. Change in behavioral performance was calculated as a difference in penalized reaction time (pRT) (2-back – 1-back) estimated in the 'Late' and 'Naive' scanning sessions.

recruitment of the ventral attention, salience, cingulo-opercular, and auditory systems ($p < 0.003$, Bonferroni corrected; Fig. 7b). In the control group, we only found increased recruitment in the auditory system. Importantly, after working memory training we also observed increased integration between salience and fronto-parietal systems, between somatomotor and auditory systems, between salience and cingulo-opercular systems, between visual and cingulo-opercular systems, between ventral attention and somatomotor systems, and between dorsal attention and cingulo-opercular systems (Fig. S7). In sensitivity and robustness analyses, we observed a similar pattern of changes in recruitment and integration when we subdivided the brain differently, using the so-called Schaefer parcellation (see **Supplementary Materials**).

DISCUSSION

In the present study, we aimed to verify the hypothesis that training on an effortful cognitive task – a dual n-back – increases the segregation of task-related functional brain networks. We examined these training-related changes utilizing both static and dynamic network approaches. While performing a dual n-back task, participants were scanned using fMRI four times: prior to training, after two weeks of training, after four weeks of training, and after six weeks of training. We examined the effect of training on whole-brain modularity, as well as on the dynamic expression of that modularity through measures of segregation and integration in task-relevant default mode and frontoparietal systems. We found that whole-brain modularity significantly differed between task conditions, being highest in the resting state, lower in the 1-back condition, and even lower in the 2-back condition. In the experimental group, modularity increased in response to working memory training. We also observed greater recruitment and lower integration of the default mode and fronto-parietal systems, suggesting enhanced intra-system communication and decremented inter-system communication. In particular, the session-dependent recruitment of the fronto-parietal system differed between control and experimental groups. The general behavioral improvement in the task in response to training was positively correlated with increased recruitment of the default mode system. Collectively, these findings suggest that dynamic communication within the default mode system supports general improvement in the task, while dynamic communication within the fronto-parietal system supports more specific network changes related to working memory training.

Modularity differences across task conditions and sessions

Modularity is a fundamental property of the organization of many complex networks including those representing transportation, social, and biological systems (Newman, 2018). The existence of modular architecture supports parallel information processing and allows the network to evolve in response to a changing environment (Simon, 1962). Together with the existence of inter-modular connections, modularity provides a basis for the emergence of segregated and integrated neuronal states in the brain (Tononi et al., 1994; Park and Friston, 2013). The balance between segregated and integrated brain states is constantly re-negotiated in the face of challenges posed by the external world (Bullmore and Sporns, 2012).

The degree of modularity in functional brain networks can change over a variety of time scales (Betzel and Bassett, 2017), from that of seconds as probed by intracranial recordings (Khambhati et al., 2017) to that of years as driven by development (Gu et al., 2015) or aging (Chan et al., 2014; Song et al., 2014; Onoda and Yamaguchi, 2013). Modularity can also be modulated

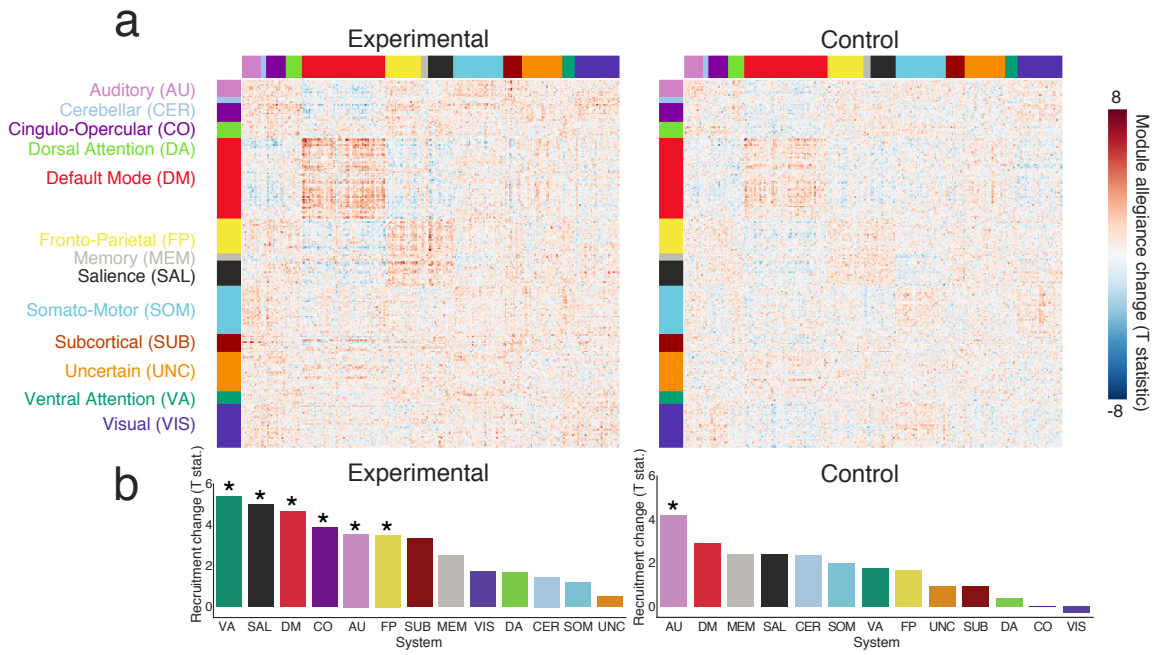

Figure 7: **Whole-brain changes in module allegiance between the 'Naive' and 'Late' stages.** (**a**) Changes in node allegiance as reflected in t-statistic values from a two-tailed t-test. (**b**) In addition to a significant increase in the default mode and fronto-parietal recruitment, the experimental group exhibited an increase in the recruitment of the ventral attention, salience, cingulo-opercular, and auditory systems ($^*p < 0.003$, Bonferroni corrected for multiple comparisons). In the control group, we only observed a significant increase in the recruitment of the auditory system.

at an intermediate temporal scale, by task demands and cognitive effort. Several studies have reported a decrease in functional brain network modularity during increasing demands on executive function, for example by varying the level of the n-back task (Kitzbichler et al., 2011; Vatansever et al., 2015; Finc et al., 2017). Here, we were curious to understand whether and how whole-brain network modularity changes when a demanding n-back task is intensively trained. We expected that network modularity would gradually increase during dual n-back task training, suggesting more segregated, and therefore less costly, information processing, after task automation.

The n-back is a classical task used to measure working memory, a primary component of executive function that broadly supports goal-directed behavior (Gallen and D'Esposito, 2019). Successful performance during the n-back task requires the participant to engage multiple cognitive processes, including encoding, storage, inhibition, and temporal ordering, as well as to execute an accurate motor response (Jonides et al., 1997). Here, in line with previous studies, we observed that modularity during the resting state was higher than during performance of the dual n-back task. Moreover, we found that the modularity during the low-demand task condition (1-back) was higher than the modularity during the high-demand task condition (2-back). Although modularity significantly increased after training in the experimental group in both conditions (1-back and 2-back), these changes did not differ significantly between the experimental and control groups. Our results are consistent with previous studies providing evidence that network segregation is lowest (while integration is highest) during a demanding n-back task, when compared to a less demanding motor task or resting state (Cohen and D'Esposito, 2016; Shine et al., 2016). Moreover, the observed difference between working memory loads is consistent with a previous study from Vatansever et al. (2015) who reported higher modularity during the 3-back condition compared to the 0-back condition, and also consistent with a previous study from Finc et al. (2017) who reported higher modularity during the 2-back condition compared to the 1-back condition. Collectively, the findings also support the Global Workspace Theory (GWT) (Dehaene et al., 1998), by showing that less demanding, highly automated tasks can be performed within segregated modules, while more challenging tasks require integration between multiple modules.

Despite the consistency between our findings and prior work, it is important to note that these previous studies did not address the question of whether a fully mastered demanding cognitive task would still require a costly integrated workspace or could instead be executed within specialized brain modules. Here, our study expands upon prior work by offering the first ev-

idence supporting the latter hypothesis. We observed that although modularity of the network generally increased through n-back training, as measured during both 1-back and 2-back conditions in the experimental group, the modularity difference between the two conditions was preserved. This finding suggests that training resulted in the increase of the baseline network segregation during the task, which supports our hypothesis that mastered cognitive tasks can be executed within a segregated network. Modularity measured during the high-demand 2-back condition after training exceeded the modularity during the low-demand 1-back condition before training. However, even if the baseline network segregation increased after the training, some level of modularity breakdown during increasing cognitive demands seems to be induced.

It is interesting to consider how this intermediate temporal scale of modular reconfiguration might relate to modular dynamics occurring at other temporal scales. Recently, Gallen and D'Esposito (2019) suggested that higher modularity of human brain functional networks can be used as a biomarker for higher cognitive plasticity during cognitive training interventions. Relatedly, Mattar et al. (2018) reported evidence that greater modularity of task-relevant systems at rest predicted the future rate of learning over 6 weeks of training. Both cognitive plasticity and the capacity to learn can change in late aging. Previous studies have demonstrated that modularity of the human brain functional networks decreases with aging, suggesting an age-related blurring of the modular structure (Chan et al., 2014; Song et al., 2014; Onoda and Yamaguchi, 2013). It would be interesting in future to examine whether there exists a significant interaction between age and the time scale of modular reconfiguration; is the decreased baseline modularity assessed at rest accompanied by a decrease or increase in dynamic modular reconfiguration during cognitively demanding tasks? And which is most predictive of behavioral performance?

Importantly, modularity is also altered in patients with disorders of mental health or patients sustaining brain injury. Studies have found that modular organization of a network is disrupted in patients with cognitive control deficits (Alexander-Bloch et al., 2010, 2012), and increases over the early stage of stroke recovery in a manner that is related to the recovery of higher cognitive functions (Siegel et al., 2018). Further longitudinal studies in these patient populations could provide clarity on the role of modularity – and its variation over a range of time scales – in higher-order cognitive function. Our findings suggest that there is a possibility to increase brain network modularity via intensive working memory training. This phenomenon may have potential beneficial implications for designing cognitive training interventions to prevent aging-related cognitive decline, reduce cognitive control deficits, or intensify effects of neurorehabilitation through increasing brain plasticity.

Increased default mode and fronto-parietal system recruitment

The modular structure of functional brain networks is not static, but instead undergoes dynamic reconfiguration throughout a range of cognitive processes (Bassett et al., 2011; Cole et al., 2013; Braun et al., 2015; Pedersen et al., 2018; He et al., 2018; Chai et al., 2016). Recently developed dynamical approaches to study brain networks are sensitive to the temporal nature of the underlying neural signal, and therefore can be used to probe the fluctuating patterns of connectivity elicited by task performance. Using just such a dynamical approach, Bassett et al. (2015) showed that the modular structure of human brain functional networks fluctuates appreciably during motor-visual learning, and moreover that the degree of fluctuations changes during a 6-week training paradigm. Task-relevant, motor and visual networks exhibited increasing autonomy as the duration of training increased, marking the emergence of automatic behavioral responses. In light of this prior work, we hypothesized that networks relevant to working memory function – including the frontoparietal and default mode systems – would increase their autonomy after extensive training on a working memory task.

In testing our hypothesis, we held in mind the observations of previous studies, which have noted that the fronto-parietal and default mode systems can both cooperate and compete during tasks that require cognitive control, such as the n-back task (Spreng et al., 2010; Cocchi et al., 2013). Understanding the nature of interactions between these two systems is therefore essential for explaining the neural adaptation that occurs in response to evolving cognitive demands. It is also not known whether dynamic interactions between these two networks may evolve during cognitive training. Here, we used a multilayer community detection algorithm to determine whether fluctuations in the modular structure of the default mode and fronto-parietal systems change in response to n-back training. Using dynamic network metrics, we showed that the default mode system increased its recruitment as training progressed, indicating that regions within this system coupled to other communities less often. The experimental and control groups did not differ significantly in the degree to which default mode recruitment increased, but they did differ in the degree to which the fronto-parietal recruitment increased, with the experimental group showing greater increases than the control group. Additionally, in both groups we observed reduced integration between the default mode and fronto-parietal systems, suggesting the existence of a trade-off between segregation and integration.

In interpreting these observations, it is useful to recall that the activity of the fronto-parietal system is

commonly linked to the performance of tasks requiring cognitive control, such as the n-back working memory task (Badre, 2008; Miller and Cohen, 2001; Vincent et al., 2008). The fronto-parietal system is comprised of spatially distributed brain areas including the lateral prefrontal cortex, anterior cingulate, and inferior parietal cortex (Vincent et al., 2008). Prior work offers evidence that the fronto-parietal system is highly flexible and dynamically interacts with other systems in response to the changing demands of cognitive tasks (Cole et al., 2013; Braun et al., 2015). In contrast, prior work frequently reports decreases in the activity of the default mode system during cognitively demanding tasks, suggesting that the system may not be consistently engaged in goal-directed cognitive processes (Shulman et al., 1997; Raichle et al., 2001). The default mode system is comprised of spatially distributed brain areas including the medial prefrontal cortex, posterior cingulate, lateral parietal cortex, and both lateral and medial temporal cortices (Buckner et al., 2008; Raichle et al., 2001). This system exhibits high activity during internally directed cognition, such as mind wandering and autobiographical memory (Buckner et al., 2008; Christoff et al., 2009).

The default mode's activity is frequently anticorrelated with the activity of systems that engage in demanding cognitive tasks such as the fronto-parietal and dorsal attention systems (Fox et al., 2005; Fransson, 2005). Some studies suggest that competitive interactions between the task-positive front-parietal system and the task-negative default mode system might be essential for higher order cognitive functions (Spreng et al., 2010; Cocchi et al., 2013). Moreover, recent evidence suggests that default mode regions may dynamically switch their connections to meet the demand of cognitive tasks and support inter-module communication (Vatansever et al., 2017; Finc et al., 2017). The location of the default mode system in the center of the macroscale cortical organization suggests that the system might indeed participate in wide-scale network integration (Margulies et al., 2016). The strength of default mode activation and functional connectivity has also previously been related to behavioral performance during working memory tasks (Hampson et al., 2006; Anticevic et al., 2010; Finc et al., 2017). Our observations expand upon these prior studies by demonstrating that the increase in default mode recruitment is positively correlated with behavioral improvement during working memory training. Taken together, more segregated default mode connectivity in response to working memory training may be an indicator of greater cognitive plasticity.

Changes in integration and recruitment beyond the default mode and fronto-parietal systems

Recent studies have provided evidence that the default mode and fronto-parietal systems may interact in a task-dependent manner with the salience, cingulo-opercular, and dorsal attention systems (Bressler and Menon, 2010; Cocchi et al., 2013; Christoff et al., 2009). Consistent with these prior observations, we demonstrated here that recruitment also increased within the salience, cingular-opercular, ventral attention, and auditory systems, particularly for the experimental group. Moreover, the salience system increased its integration with the fronto-parietal system and with the cingulo-opercular system, while the cingulo-opercular system increased its integration with the dorsal attention system. A similar pattern of changes was observed across two different subdivisions of the cortex into systems (Power and Schaefer), collectively suggesting that the salience and cingulo-opercular systems that are thought to be responsible for switching between antagonistic fronto-parietal and default mode systems, appear to be more integrated with the fronto-parietal system and less integrated with the default mode system. This pattern of relations may be due to diminished requirements for switching between these two systems when the task is well learned.

CONCLUSIONS

Dynamic adaptation of the functional networks in the central nervous system occurs across multiple time scales. Our results demonstrate that adult human brain functional networks not only reorganize during a working memory task, but also can be modulated by the level of expertise in the task. After working memory training, brain networks are more segregated. The increase in segregation is visible at the whole-brain level for static networks, and also evidenced by increased task-relevant system recruitment when considering dynamic networks composed of task blocks. Together, these results shed new light on the mechanisms underlying brain network reorganization accompanying the automation of performance on cognitively demanding tasks.

METHODS

Subjects

Fifty-three healthy volunteers (26 female; mean age: 21.17; age range: 18–28 years) were recruited from the local community through word-of-mouth and social networks. All participants were right-handed, had normal or corrected-to-normal vision, and had no hearing deficits. Seven participants did not complete the study: one due to brain structure abnormalities detected at the first scanning session, and six due to not completing

the training procedure. The final sample consisted of forty-six participants who completed the entire training procedure, participated in all four fMRI scanning sessions, and had no history of neurological or psychiatric disorders nor gross brain structure abnormalities. After the first fMRI scan, participants were matched by sex and randomly assigned to one of the two training groups: experimental and control (see next section on "Experimental Procedures"). Each group consisted of 23 subjects with no group differences in age (two-sample t-test: $t(42.839) = 0.22$, $p = 0.83$) or fluid intelligence (two-sample t-test: $t(42.882) = 0.51$, $p = 0.61$) as measured by Raven's Advanced Progressive Matrices (RAPM) (Raven and Raven's Progressive Matrices, 1994). Informed consent was obtained in writing from each participant, and ethical approval for the study was obtained from the Ethics Committee of the Nicolaus Copernicus University Ludwik Rydygier Collegium Medicum in Bydgoszcz, Poland, in accordance with the Declaration of Helsinki.

Experimental Procedures

The study was performed at the Centre for Modern Interdisciplinary Technologies, Nicolaus Copernicus University in Toruń (Poland). Each participant who completed the entire study procedure attended a total of 24 meetings at the laboratory. During the first meeting, participants were familiarized with the study procedure and timeline, and were asked to provide basic demographic information and informed consent. During the second meeting, participants performed fluid intelligence testing with RAMP (Raven and Raven's Progressive Matrices, 1994). Then, participants were scheduled for fMRI testing, which was performed before training, after two weeks of training, after four weeks of training, and after 6 weeks of training. Each fMRI session was scheduled to be on the same day of the week and at the same hour for each participant. These schedules varied in exceptional cases (holidays, illness of participant, emergency). However, scanning procedures were always performed between 24h to 48h after the last training session. After the first fMRI session, participants were randomly assigned to one of two training groups: (1) experimental, which trained working memory with an adaptive dual n-back task (Jaeggi et al., 2008), and (2) a passive control group which interchangeably performed an auditory and spatial 1-back task. We included this second group to control for differences in the effect of training on task performance and fMRI signatures driven by repeated exposure to a task.

The dual n-back task performed by the experimental group consisted of visuospatial and auditory tasks performed simultaneously. Visuospatial stimuli consisted of 8 blue squares presented sequentially on the 3×3 grid with a white fixation cross in the middle of the black screen; auditory stimuli consisted of 8 Polish consonants (b, k, w, s, r, g, n, z) played sequentially in headphones. Participants were asked to indicate by pressing a button with their left index finger whether the letter heard through the headphones was the same as the letter n-back in the sequence, and by pressing a button with their right index finger to indicate whether the square on the screen was in the same location as the square n-back in the sequence. The n level of the dual n-back task increased adaptively when participants achieved 80% correct responses in the trial, and the n level decreased when participants made more than 50% errors in the trial. After each trial, the n level achieved by a participant was recorded, and the mean n level during each of 18 training session was used later to calculate the total training progress. Participants from the control group performed a single 1-back with auditory or visuospatial stimuli variants. To minimize boredom of participants, the order of the 1-back variants was randomly selected at the beginning of each training session. Therefore, each participant from the control group had the same number of training trials on single auditory and visuospatial n-back tasks.

Participants completed a total of 18 sessions (30 min each) under the supervision of the experimenter. Each participant completed 20 blocks (each consisting of 20 + n trials, depending on the n level achieved by the participant) of the n-back task during each training session. The study was double-blind; the experimenter performing the fMRI examination was not aware of the group assignment of the participants, and participants were not aware that the study was designed in a way that there were two groups (experimental and control). The apparatus used in the study consisted of two 17" Dell Inspiron Laptops, and two pairs of Sennheiser headphones. Stimulus delivery was controlled by a Python adaptation of the dual n-back task used by Jaeggi et al. (2008) (`http://brainworkshop.sourceforge.net/`). All participants received equal monetary remuneration (200 PLN) for study participation together with a radiological description and a CD containing their anatomical brain scans.

Data acquisition

Neuroimaging data were collected using a GE Discovery MR750 3 Tesla MRI scanner (General Electric Healthcare) with a standard 8-channel head coil. Structural images were collected using a three-dimensional high resolution T1-weighted gradient-echo (FSPGR BRAVO) sequence (TR = 8.2 s, TE = 3.2 ms, FOV = 256 mm, flip angle = 12 degrees, matrix size 256×256, voxel size = $1 \times 1 \times 1$ mm, 206 axial oblique slices). Functional scans were obtained using a T2*-weighted gradient-echo, echo- planar imaging (EPI) sequence sensitive to BOLD contrast (TR = 2,000 ms, TE = 30 ms, FOV = 192 mm, flip angle = 90 degrees, ma-

trix size = 64 × 64, voxel size 3 × 3 × 3 mm, 0.5 mm gap). For each functional run, 42 axial oblique slices were acquired in an interleaved acquisition scheme, and 5 dummy scans (10 s) were obtained to stabilize magnetization at the beginning of the EPI sequence. Resting state (10 min 10 s, 305 volumes) data was acquired at the beginning of each scanning session. During the resting state, participants were asked to focus their eyes on the fixation cross in the middle of the screen. Then, during the dual n-back task (11 min 30 s; 340 volumes), participants simultaneously performed two versions of the task: spatial and auditory. During the spatial version, blue squares were presented sequentially for 500 ms on the screen in one of the 8 different locations on a 3 × 3 grid. A fixation cross was displayed at the center of the plane during each block of the experiment. During the auditory version, 8 polish consonants (b, k, w, s, r, g, n, z) were played sequentially in headphones. Each session of the task consisted of 20 blocks (30 s per block; 12 trials with 25% of targets) of alternating 1- and 2-back conditions. The instruction screen was displayed for 4,000 ms before each block, informing the participant of the upcoming condition. Both visual and auditory stimuli were presented in a pseudo-random order.

Participants were asked to push the button with their right thumb if the currently presented square was in the same location as the previous square (1-back) or two squares back in the sequence (2-back) and, at the same time, push the button with their left thumb when the currently played consonant was the same as the previous consonant (1-back) or two consonants back (2-back). The participants had 2,000 ms to respond, and were instructed to respond as quickly and accurately as possible. The experimental protocol execution and control (stimulus delivery and response registration) employed version 17.2. of Presentation software (Neurobehavioral Systems, Albany, NY), as well as MRI compatible goggles (visual stimulation), headphones (auditory stimulation), and response grips (response registration) (NordicNeuroLab, Bergen, Norway). Before each scanning session, participants performed a short dual n-back training session outside the fMRI scanner to (re-)familiarize them with the rules of the task.

Behavioral performance

To measure behavioral performance in the dual n-back scanning sessions, we incorporated *penalized reaction time* (pRT), which is a measure previously introduced by Ginestet and Simmons (2011). This measure combines both measures of accuracy and response time. For every subject, session, task condition, and stimulus modality (auditory, spatial), pRT was defined as:

$$pRT = \frac{1}{n}\sum_{i=1} x_i, \tag{1}$$

where the index i denotes all possible responses, and x_i is obtained from the following formula:

$$x_i = \begin{cases} RT_i, \text{ if subject answered correctly} \\ 2000, \text{ otherwise,} \end{cases} \tag{2}$$

where RT_i is reaction time of the response during the i-th trial and the scalar value of 2000 is a penalty for an incorrect answer or for the lack of an answer, which is the maximum possible time to respond during each n-back trial measured in milliseconds. For each participant, we calculated average pRT for both modalities to represent a cumulative measure of performance during the dual n-back task.

Data processing

After converting from DICOM to NifTI format, functional and anatomical data were structured according to the BIDS (Brain Imaging Data Structure) standard (Gorgolewski et al., 2016) and validated with BIDS Validator (`https://bids-standard.github.io/bids-validator/`).

Neuroimaging data was preprocessed using fMRIPrep 1.1.1 (Esteban et al., 2018) a Nipype (Gorgolewski et al., 2011, 2017) based tool. Each T1w (T1-weighted) volume was corrected for INU (intensity non-uniformity) using N4BiasFieldCorrection v2.1.0 (Tustison et al., 2010) and skull-stripped using antsBrainExtraction.sh v2.1.0 (employing the OASIS template). Brain surfaces were reconstructed using recon-all from FreeSurfer v6.0.1 (Dale et al., 1999), and the brain mask estimated previously was refined with a custom variation of the method to reconcile ANTs-derived and FreeSurfer-derived segmentations of the cortical gray-matter of Mindboggle (Klein et al., 2017). Spatial normalization to the ICBM 152 Nonlinear Asymmetrical template version 2009c (Fonov et al., 2009) was performed through nonlinear registration with the antsRegistration tool of ANTs v2.1.0 (Avants et al., 2008), using brain-extracted versions of both the T1w volume and template. Brain tissue segmentation of cerebrospinal fluid (CSF), white matter (WM), and gray matter was performed on the brain-extracted T1w using FAST (Zhang et al., 2001)(FSL v5.0.9).

Functional data was slice time corrected using 3dTshift from AFNI v16.2.07 (Cox, 1996) and motion corrected using MCFLIRT (FSL v5.0.9, Jenkinson et al. (2002). This process was followed by co-registration to the corresponding T1w using boundary-based registration (Greve and Fischl, 2009) with 9 degrees of freedom, using bbregister (FreeSurfer v6.0.1). Motion correcting transformations, BOLD-to-T1w transformation and T1w-to-template (MNI) warp were concatenated and applied in a single step using antsApplyTransforms (ANTs v2.1.0) employing Lanczos interpolation.

Physiological noise regressors were extracted by applying CompCor (Behzadi et al., 2007). Principal com-

ponents were estimated for the two CompCor variants: temporal (tCompCor) and anatomical (aCompCor). A mask to exclude signal with cortical origin was obtained by eroding the brain mask, ensuring that it only contained subcortical structures. Six tCompCor components were then calculated including only the top 5% variable voxels within that subcortical mask. For aCompCor, six components were calculated within the intersection of the subcortical mask and the union of the CSF and WM masks calculated in T1w space, after their projection to the native space of each functional run. Frame-wise displacement (FD, Power et al. (2014) was calculated for each functional run using the implementation of Nipype. The internal operations of fMRIPrep use Nilearn (Abraham et al., 2014), principally within the BOLD-processing workflow. For more details of the pipeline see `https://fmriprep.readthedocs.io/en/latest/workflows.html`.

Non-smoothed functional images were denoised using Nilearn (Abraham et al., 2014) and Nistats. We implemented voxel-wise confound regression by regressing out (1) signals from six aCompCor components, (2) 24 motion parameters representing 3 translation and 3 rotation timecourses, their temporal derivatives, and quadratic terms of both, (3) outlier frames with FD $>$ 0.5mm and DVARS (Derivative of rms VARiance over voxelS) (Power et al., 2012) with a threshold of $\pm$ 3 SD, together with their temporal derivatives, (4) task effects and their temporal derivatives (Whitfield-Gabrieli and Nieto-Castanon, 2012), and (5) any general linear trend.

Functional connectivity estimation

Functional connectivity is a measure of the statistical relation between time-series of spatially distinct brain regions. Time-series can be defined as signals from single voxels or as the mean of the signals from anatomically or functionally defined groups of voxels, also known as brain parcels (Eickhoff et al., 2018). Here, we used a functional brain parcellation comprised of 264 regions of interests (ROIs) provided by Power et al. (2011). This parcellation was based on meta-analysis and has previously been used in many studies focused on task-based network reorganization (Cole et al., 2013; Vatansever et al., 2015; Finc et al., 2017). To validate our results, we also used a 300-ROI parcellation provided by Schaefer et al. (2017), which is based on transitions of functional connectivity patterns.

We created $N \times N$ correlation matrices by calculating the Pearson's correlation coefficient between the mean signal time-course of region i and the mean signal time-course of region j, for all pairs of ROIs (i,j). We retained only positive correlations for further analysis. In the case of the dual n-back task, we employed a weighted correlation measure, to control for delays due to the hemodynamic response function (HRF) (Whitfield-Gabrieli and Nieto-Castanon, 2012). In this procedure, we first convolved task block regressors with the HRF and applied a filter to retain only positive values of the resultant time-series. Then, original time-series were filtered according to the task condition and positive values of the HRF-convolved time-series. Next, the weighted correlation coefficient was calculated between the concatenated block time series, with weights taken from the corresponding HRF-convolved signals. Finally, Fisher's transformation was employed to convert Pearson's correlation coefficients to normally distributed z-scores. This procedure resulted in 264×264 (Power parcellation) and 300×300 (Schaefer parcellation) correlation matrices for each subject, session, and task condition (resting-state, 1-back, 2-back). For the dynamic network analyses, we calculated the weighted correlations for each block of the n-back task, resulting in $264 \times 264 \times 20$ and $300 \times 300 \times 20$ matrices, where the third dimension represents the number of task blocks (20 interleaved blocks of 1-back and 2-back).

Static modularity

To calculate the extent of whole-brain network segregation, we employed a Louvain-like community detection algorithm (Blondel et al., 2008) to optimize a common modularity quality function (Newman and Girvan, 2004). This algorithm partitions the network into communities, where nodes in a given community are highly interconnected among themselves, and sparsely interconnected to the rest of the network. The modularity quality index, Q, to be optimized was defined as follows:

$$Q_S = \frac{1}{2\mu} \sum_{ij} (A_{ij} - \gamma V_{ij}) \delta(g_i, g_j), \tag{3}$$

where $\mu = \frac{1}{2} \sum_{ij} A_{ij}$ is the total edge weight of the network, A_{ij} is the strength of the edge between node i and node j, and γ is the structural resolution parameter. The Kronecker delta function $\delta(g_i, g_j)$ equals one if nodes i and j belong to the same module, and equals zero otherwise. The term V_{ij} represents the connectivity strength expected by chance in the configuration null model:

$$V_{ij} = \frac{k_i k_j}{2m}, \tag{4}$$

where k_i and k_j are the weighted degrees of nodes i and j, respectively, and $m = \frac{1}{2} \sum_{ij} A_{ij}$ is the sum of all nodal weighted degrees.

Since the Louvain algorithm is non-deterministic, we run it 100 times, and then consider the network partition with the highest modularity score across these runs. It is important to note that the values of graph theoretical metrics can vary markedly depending on the sum of connection strengths in the network (Rubinov and Sporns, 2011; Fornito et al., 2016). To take this

effect into account, we normalized each individual modularity value against a set of modularity values calculated for randomly rewired networks Maslov and Sneppen (2002). For this purpose, we created 100 null networks using random rewiring of each original functional network. Then, modularity scores were calculated for each null network, thereby creating a null distribution. Finally, we normalized modularity values by dividing them by the mean of the corresponding null distribution.

Multilayer modularity

To calculate measures of recruitment and integration, we performed multilayer modularity maximization used a generalized Louvain-like community detection algorithm introduced by Mucha et al. (2010). This algorithm allows the optimization of a modularity quality function on a network with multiple layers. In our study, networks calculated for each separate block were considered as consecutive layers of the multilayer network. For each subject, session, and multilayer network, we ran 100 optimizations of the modularity quality function, defined as:

$$Q_{ML} = \frac{1}{2\mu}\sum_{ijsr}[(A_{ijs} - \gamma_s V_{ijs})\delta_{sr} + \delta_{ij}\omega_{sr}]\delta(g_{is}, g_{ir}), \tag{5}$$

where A_{ijs} represents the element of the adjacency matrix at slice s, V_{ijs} represents the element of the null model matrix at slice s, g_{ir} provides the community assignment of node i in slice r, $\mu = \frac{1}{2}\sum_{ij}\kappa_{jr}$ is the total edge weight of the network, where $\kappa_{js} = k_{js} + c_{js}$ is the strength of node j in slice s, the k_{js} is the interslice strength of node j in slice s, and $c_{js} = \sum_r \omega_{jsr}$. For all slices we used the Newman-Girvan null model, also known as the configuration model, defined as:

$$V_{ijs} = \frac{k_{is}k_{js}}{2m_s}, \tag{6}$$

where $m_s = \frac{1}{2}\sum_{ij} A_{ijs}$ is the total edge weight of slice s. In this optimization, there are two free-parameters: γ_s and ω_{jsr}. The parameter γ_s is the structural resolution parameter for slice s, and the parameter ω_{isr} represents the connection strength between node j in slice s and node j in slice r. These two parameters can be used to tune the size of communities within each layer and the number of communities detected across all layers, respectively. Here, in line with previous studies we set $\gamma = 1$ (Mattar et al., 2015). Due to the interleaved nature of our experimental design, $\omega = 1$ for slices from the same task condition, and $\omega = 0.5$ for slices from different task conditions.

Network diagnostics

Multilayer community detection results in a single module assignment $N \times T$ matrix, where each matrix element represents the module assignment of a given node for a given slice. To summarize the dynamics of module assignments for each subject and session, we calculated an $N \times N$ module allegiance matrix, P, where the element P_{ij} represents the fraction of network layers for which node i and node j belong to the same community (Mattar et al., 2015; Bassett et al., 2015):

$$P_{ij} = \frac{1}{OT}\sum_{o=1}^{O}\sum_{t=1}^{T} a_{i,j}^{k,o}, \tag{7}$$

where O is the number of repetitions of the multilayer community detection algorithm (here, $O = 100$), and T is the number of slices (here 20 task blocks). For each optimization o and slice t,

$$a_{i,j}^{k,o} = \begin{cases} 0, \text{ if nodes } i \text{ and } j \text{ are in the same module} \\ 1, \text{ otherwise.} \end{cases} \tag{8}$$

To characterize the dynamics of default mode and frontoparietal system recruitment and integration, we employed methods of functional cartography (Mattar et al., 2015; Bassett et al., 2015). These measures allow us to summarize how often regions from the system of interest are assigned to the same module. We can define the recruitment of system S as:

$$R_S = \frac{1}{n_S^2}\sum_{i\in S}\sum_{j\in S} P_{i,j}. \tag{9}$$

The recruitment of system S is high when regions within the system tend to be assigned to the same module throughout all task blocks. Similarly, we can define the integration coefficient between system S_k and system S_l as:

$$I_{S_k S_l} = \frac{1}{n_{S_k} n_{S_l}}\sum_{i\in S_k}\sum_{j\in S_l} P_{ij}. \tag{10}$$

Systems of interest are highly integrated when regions belonging to two different systems are frequently assigned to the same community.

Statistical modeling

Due to the nested nature of the study data, we used two-level (trials nested within participants) and three-level (trials nested within sessions nested within participants) multilevel models (MLM; Snijders and Bosker (2012)) at four points during our analysis of the data. In all cases, random intercepts were estimated. The significance of models was estimated with chi-square tests, where models with increasing complexity were compared and the resulting value of Likelihood Ratio Test (χ^2) and corresponding p-value were reported (Field et al., 2012).

Behavioral changes during training. To investigate behavioral changes in penalized reaction time (pRT) depending on the session, task condition, and group,

we used a three-level multilevel model with pRT as the dependent variable and with group (2 factors: experimental and control), condition (2 factors: 1-back and 2-back, reference category: 1-back), and session (4 factors: Naive, Early Middle, Late; reference category: Naive) as independent variables. In addition to the main effects (group, condition, session), we included the following interaction terms: group × session, condition × session, group × condition, and group × condition × session.

Modularity at baseline. To investigate the dependence of static modularity at baseline on task condition, we used a two-level multilevel model with static modularity as the dependent variable and with task condition (3 factors: rest, 1-back, 2-back, two orthogonal contrasts: rest vs. 1-back and 2-back, 1-back vs. 2-back) as the independent variable. The main effect of condition was tested.

Training-dependent changes in static modularity. To investigate the dependence of static modularity on the session, task condition, and group, we used a three-level multilevel model with static modularity as the dependent variable and with group (2 factors: experimental and control), condition (2 factors: 1-back and 2-back), and session (4 factors: Naive, Early Middle, Late, reference category: Naive) as independent variables. In addition to the main effects (group, condition, session), we included the following interaction terms: group × session, condition × session, group × condition, and group × condition × session.

Changes in dynamic network metrics. To investigate default mode recruitment, fronto-parietal recruitment, and the integration between the default mode and fronto-parietal systems, we used a two-level multilevel model with the diagnostic measure (recruitment/integration) as the dependent variable and with group (2 factors: experimental and control) and session (4 factors: Naive, Early Middle, Late, reference category: Naive) as independent variables. In addition to the main effects (group, session), we included the following interaction term: group × session.

Relationship between the change in default mode and fronto-parietal recruitment and the improvement in behavior. We also used multilevel modeling to investigate differences in the slope of the relationship between the change in recruitment and the change in behavior. Here we examined the relationship between two variables: Δ of system recruitment (change from Naive to Late) and Δ of behavioral performance (change from Naive to Late). We compared the slope of this relationship between the two groups (2 factors: experimental and control).

Code and data availability

All code used for neuroimaging and behavioral data processing, statistical data analyses, as well as processed data are publicly available at `https://osf.io/wf85u/` (DOI 10.17605/OSF.IO/WF85U). The raw data analyzed in the current study are available from the corresponding author on request.

ACKNOWLEDGMENTS

The study was supported by the National Science Centre, Poland (2015/17/N/HS6/03549). K.F. was supported by National Science Centre, Poland (2015/17/N/HS6/03549, 2017/24/T/HS6/00105) and Foundation for Polish Science, Poland (START 23.2018). Calculations have been carried out using resources provided by Wroclaw Centre for Networking and Supercomputing (`http://wcss.pl`), grant No. 467. D.S.B. also acknowledges support from the John D. and Catherine T. MacArthur Foundation, the Alfred P. Sloan Foundation, the ISI Foundation, the Paul Allen Foundation, the Army Research Laboratory (W911NF-10-2-0022), the Army Research Office (Bassett-W911NF-14-1-0679, Grafton-W911NF-16-1-0474, DCIST- W911NF-17-2-0181), the Office of Naval Research, the National Institute of Mental Health (2-R01-DC-009209-11, R01-MH112847, R01-MH107235, R21-M MH-106799), the National Institute of Child Health and Human Development (1R01HD086888-01), the National Institute of Neurological Disorders and Stroke (R01 NS099348), and the National Science Foundation (BCS-1441502, BCS-1430087, NSF PHY-1554488 and BCS-1631550). We also thank Maja Dobija, Alex Lubiński, Stanisław Narębski, Monika Muchlado, Bożena Pięta, and Adrianna Przybysz for their assistance in conducting training sessions, and Jaromir Patyk for technical support. The content is solely the responsibility of the authors and does not necessarily represent the official views of any of the funding agencies.

References

Abraham, A., Pedregosa, F., Eickenberg, M., Gervais, P., Mueller, A., Kossaifi, J., Gramfort, A., Thirion, B., and Varoquaux, G. (2014). Machine learning for neuroimaging with scikit-learn. *Frontiers in neuroinformatics*, 8:14.

Alexander-Bloch, A., Lambiotte, R., Roberts, B., Giedd, J., Gogtay, N., and Bullmore, E. (2012). The discovery of population differences in network community structure: new methods and applications to brain functional networks in schizophrenia. *Neuroimage*, 59(4):3889–3900.

Alexander-Bloch, A. F., Gogtay, N., Meunier, D., Birn, R., Clasen, L., Lalonde, F., Lenroot, R., Giedd, J., and Bullmore, E. T. (2010). Disrupted modularity and local connectivity of brain functional networks

in childhood-onset schizophrenia. *Frontiers in systems neuroscience*, 4:147.

Anticevic, A., Repovs, G., Shulman, G. L., and Barch, D. M. (2010). When less is more: Tpj and default network deactivation during encoding predicts working memory performance. *Neuroimage*, 49(3):2638–2648.

Avants, B. B., Epstein, C. L., Grossman, M., and Gee, J. C. (2008). Symmetric diffeomorphic image registration with cross-correlation: evaluating automated labeling of elderly and neurodegenerative brain. *Medical image analysis*, 12(1):26–41.

Badre, D. (2008). Cognitive control, hierarchy, and the rostro–caudal organization of the frontal lobes. *Trends in cognitive sciences*, 12(5):193–200.

Bassett, D. S., Wymbs, N. F., Porter, M. A., Mucha, P. J., Carlson, J. M., and Grafton, S. T. (2011). Dynamic reconfiguration of human brain networks during learning. *Proceedings of the National Academy of Sciences*.

Bassett, D. S., Wymbs, N. F., Rombach, M. P., Porter, M. A., Mucha, P. J., and Grafton, S. T. (2013). Task-based core-periphery organization of human brain dynamics. *PLoS computational biology*, 9(9):e1003171.

Bassett, D. S., Yang, M., Wymbs, N. F., and Grafton, S. T. (2015). Learning-induced autonomy of sensorimotor systems. *Nature neuroscience*, 18(5):744.

Behzadi, Y., Restom, K., Liau, J., and Liu, T. T. (2007). A component based noise correction method (compcor) for bold and perfusion based fmri. *Neuroimage*, 37(1):90–101.

Betzel, R. F. and Bassett, D. S. (2017). Multi-scale brain networks. *Neuroimage*, 160:73–83.

Betzel, R. F., Byrge, L., He, Y., Goñi, J., Zuo, X.-N., and Sporns, O. (2014). Changes in structural and functional connectivity among resting-state networks across the human lifespan. *Neuroimage*, 102:345–357.

Blondel, V. D., Guillaume, J.-L., Lambiotte, R., and Lefebvre, E. (2008). Fast unfolding of communities in large networks. *Journal of statistical mechanics: theory and experiment*, 2008(10):P10008.

Braun, U., Schäfer, A., Walter, H., Erk, S., Romanczuk-Seiferth, N., Haddad, L., Schweiger, J. I., Grimm, O., Heinz, A., Tost, H., et al. (2015). Dynamic reconfiguration of frontal brain networks during executive cognition in humans. *Proceedings of the National Academy of Sciences*, 112(37):11678–11683.

Bressler, S. L. and Menon, V. (2010). Large-scale brain networks in cognition: emerging methods and principles. *Trends in cognitive sciences*, 14(6):277–290.

Buckner, R. L., Andrews-Hanna, J. R., and Schacter, D. L. (2008). The brain's default network. *Annals of the New York Academy of Sciences*, 1124(1):1–38.

Bullmore, E. and Sporns, O. (2012). The economy of brain network organization. *Nature Reviews Neuroscience*, 13(5):336.

Chai, L. R., Mattar, M. G., Blank, I. A., Fedorenko, E., and Bassett, D. S. (2016). Functional network dynamics of the language system. *Cerebral Cortex*, 26(11):4148–4159.

Chan, M. Y., Park, D. C., Savalia, N. K., Petersen, S. E., and Wig, G. S. (2014). Decreased segregation of brain systems across the healthy adult lifespan. *Proceedings of the National Academy of Sciences*, 111(46):E4997–E5006.

Christoff, K., Gordon, A. M., Smallwood, J., Smith, R., and Schooler, J. W. (2009). Experience sampling during fmri reveals default network and executive system contributions to mind wandering. *Proceedings of the National Academy of Sciences*, 106(21):8719–8724.

Cocchi, L., Zalesky, A., Fornito, A., and Mattingley, J. B. (2013). Dynamic cooperation and competition between brain systems during cognitive control. *Trends in cognitive sciences*, 17(10):493–501.

Cohen, J. R. and D'Esposito, M. (2016). The segregation and integration of distinct brain networks and their relationship to cognition. *Journal of Neuroscience*, 36(48):12083–12094.

Cole, M. W., Reynolds, J. R., Power, J. D., Repovs, G., Anticevic, A., and Braver, T. S. (2013). Multi-task connectivity reveals flexible hubs for adaptive task control. *Nature Neuroscience*, 16(9):1348.

Cox, R. W. (1996). Afni: software for analysis and visualization of functional magnetic resonance neuroimages. *Computers and Biomedical research*, 29(3):162–173.

Dale, A. M., Fischl, B., and Sereno, M. I. (1999). Cortical surface-based analysis: I. segmentation and surface reconstruction. *Neuroimage*, 9(2):179–194.

Dehaene, S., Kerszberg, M., and Changeux, J.-P. (1998). A neuronal model of a global workspace in effortful cognitive tasks. *Proceedings of the National Academy of Sciences*, 95(24):14529–14534.

Eickhoff, S. B., Yeo, B. T., and Genon, S. (2018). Imaging-based parcellations of the human brain. *Nature Reviews Neuroscience*, page 1.

Esteban, O., Markiewicz, C., Blair, R. W., Moodie, C., Isik, A. I., Aliaga, A. E., Kent, J., Goncalves, M., DuPre, E., Snyder, M., et al. (2018). Fmriprep:

a robust preprocessing pipeline for functional mri. *bioRxiv*, page 306951.

Field, A., Miles, J., and Field, Z. (2012). *Discovering statistics using R*. Sage publications.

Finc, K., Bonna, K., Lewandowska, M., Wolak, T., Nikadon, J., Dreszer, J., Duch, W., and Kühn, S. (2017). Transition of the functional brain network related to increasing cognitive demands. *Human brain mapping*, 38(7):3659–3674.

Fonov, V. S., Evans, A. C., McKinstry, R. C., Almli, C., and Collins, D. (2009). Unbiased nonlinear average age-appropriate brain templates from birth to adulthood. *NeuroImage*, (47):S102.

Fornito, A., Zalesky, A., and Bullmore, E. (2016). *Fundamentals of brain network analysis*. Academic Press.

Fox, M. D., Snyder, A. Z., Vincent, J. L., Corbetta, M., Van Essen, D. C., and Raichle, M. E. (2005). The human brain is intrinsically organized into dynamic, anticorrelated functional networks. *Proceedings of the National Academy of Sciences*, 102(27):9673–9678.

Fransson, P. (2005). Spontaneous low-frequency bold signal fluctuations: An fmri investigation of the resting-state default mode of brain function hypothesis. *Human brain mapping*, 26(1):15–29.

Friston, K. J. (2009). Modalities, modes, and models in functional neuroimaging. *Science*, 326(5951):399–403.

Gallen, C. L. and D'Esposito, M. (2019). Brain modularity: A biomarker of intervention-related plasticity. *Trends in cognitive sciences*.

Ginestet, C. E. and Simmons, A. (2011). Statistical parametric network analysis of functional connectivity dynamics during a working memory task. *Neuroimage*, 55(2):688–704.

Gorgolewski, K., Burns, C. D., Madison, C., Clark, D., Halchenko, Y. O., Waskom, M. L., and Ghosh, S. S. (2011). Nipype: a flexible, lightweight and extensible neuroimaging data processing framework in python. *Frontiers in neuroinformatics*, 5:13.

Gorgolewski, K. J., Auer, T., Calhoun, V. D., Craddock, R. C., Das, S., Duff, E. P., Flandin, G., Ghosh, S. S., Glatard, T., Halchenko, Y. O., et al. (2016). The brain imaging data structure, a format for organizing and describing outputs of neuroimaging experiments. *Scientific Data*, 3:160044.

Gorgolewski, K. J., Esteban, O., Ellis, D. G., Notter, M. P., Ziegler, E., Johnson, H., Hamalainen, C., Yvernault, B., Burns, C., Manhães-Savio, A., Jarecka, D., Markiewicz, C. J., Salo, T., Clark, D., Waskom, M., Wong, J., Modat, M., Dewey, B. E., Clark, M. G., Dayan, M., Loney, F., Madison, C., Gramfort, A., Keshavan, A., Berleant, S., Pinsard, B., Goncalves, M., Clark, D., Cipollini, B., Varoquaux, G., Wassermann, D., Rokem, A., Halchenko, Y. O., Forbes, J., Moloney, B., Malone, I. B., Hanke, M., Mordom, D., Buchanan, C., Pauli, W. M., Huntenburg, J. M., Horea, C., Schwartz, Y., Tungaraza, R., Iqbal, S., Kleesiek, J., Sikka, S., Frohlich, C., Kent, J., Perez-Guevara, M., Watanabe, A., Welch, D., Cumba, C., Ginsburg, D., Eshaghi, A., Kastman, E., Bougacha, S., Blair, R., Acland, B., Gillman, A., Schaefer, A., Nichols, B. N., Giavasis, S., Erickson, D., Correa, C., Ghayoor, A., Küttner, R., Haselgrove, C., Zhou, D., Craddock, R. C., Haehn, D., Lampe, L., Millman, J., Lai, J., Renfro, M., Liu, S., Stadler, J., Glatard, T., Kahn, A. E., Kong, X.-Z., Triplett, W., Park, A., McDermottroe, C., Hallquist, M., Poldrack, R., Perkins, L. N., Noel, M., Gerhard, S., Salvatore, J., Mertz, F., Broderick, W., Inati, S., Hinds, O., Brett, M., Durnez, J., Tambini, A., Rothmei, S., Andberg, S. K., Cooper, G., Marina, A., Mattfeld, A., Urchs, S., Sharp, P., Matsubara, K., Geisler, D., Cheung, B., Floren, A., Nickson, T., Pannetier, N., Weinstein, A., Dubois, M., Arias, J., Tarbert, C., Schlamp, K., Jordan, K., Liem, F., Saase, V., Harms, R., Khanuja, R., Podranski, K., Flandin, G., Papadopoulos Orfanos, D., Schwabacher, I., McNamee, D., Falkiewicz, M., Pellman, J., Linkersdörfer, J., Varada, J., Pérez-García, F., Davison, A., Shachnev, D., and Ghosh, S. (2017). Nipype: a flexible, lightweight and extensible neuroimaging data processing framework in Python. 0.13.1.

Greve, D. N. and Fischl, B. (2009). Accurate and robust brain image alignment using boundary-based registration. *Neuroimage*, 48(1):63–72.

Gu, S., Satterthwaite, T. D., Medaglia, J. D., Yang, M., Gur, R. E., Gur, R. C., and Bassett, D. S. (2015). Emergence of system roles in normative neurodevelopment. *Proceedings of the National Academy of Sciences*, 112(44):13681–13686.

Hampson, M., Driesen, N. R., Skudlarski, P., Gore, J. C., and Constable, R. T. (2006). Brain connectivity related to working memory performance. *Journal of Neuroscience*, 26(51):13338–13343.

He, X., Bassett, D. S., Chaitanya, G., Sperling, M. R., Kozlowski, L., and Tracy, J. I. (2018). Disrupted dynamic network reconfiguration of the language system in temporal lobe epilepsy. *Brain*, 141(5):1375–1389.

Jaeggi, S. M., Buschkuehl, M., Jonides, J., and Perrig, W. J. (2008). Improving fluid intelligence with training on working memory. *Proceedings of the National Academy of Sciences*, 105(19):6829–6833.

Jenkinson, M., Bannister, P., Brady, M., and Smith, S. (2002). Improved optimization for the robust and accurate linear registration and motion correction of brain images. *Neuroimage*, 17(2):825–841.

Jonides, J., Schumacher, E. H., Smith, E. E., Lauber, E. J., Awh, E., Minoshima, S., and Koeppe, R. A. (1997). Verbal working memory load affects regional brain activation as measured by pet. *Journal of cognitive neuroscience*, 9(4):462–475.

Khambhati, A. N., Bassett, D. S., Oommen, B. S., Chen, S. H., Lucas, T. H., Davis, K. A., and Litt, B. (2017). Recurring functional interactions predict network architecture of interictal and ictal states in neocortical epilepsy. *eNeuro*, 4(1).

Kitzbichler, M. G., Henson, R. N., Smith, M. L., Nathan, P. J., and Bullmore, E. T. (2011). Cognitive effort drives workspace configuration of human brain functional networks. *Journal of Neuroscience*, 31(22):8259–8270.

Klein, A., Ghosh, S. S., Bao, F. S., Giard, J., Häme, Y., Stavsky, E., Lee, N., Rossa, B., Reuter, M., Neto, E. C., et al. (2017). Mindboggling morphometry of human brains. *PLoS computational biology*, 13(2):e1005350.

Margulies, D. S., Ghosh, S. S., Goulas, A., Falkiewicz, M., Huntenburg, J. M., Langs, G., Bezgin, G., Eickhoff, S. B., Castellanos, F. X., Petrides, M., et al. (2016). Situating the default-mode network along a principal gradient of macroscale cortical organization. *Proceedings of the National Academy of Sciences*, 113(44):12574–12579.

Maslov, S. and Sneppen, K. (2002). Specificity and stability in topology of protein networks. *Science*, 296(5569):910–913.

Mattar, M. G., Cole, M. W., Thompson-Schill, S. L., and Bassett, D. S. (2015). A functional cartography of cognitive systems. *PLoS computational biology*, 11(12):e1004533.

Mattar, M. G., Wymbs, N. F., Bock, A. S., Aguirre, G. K., Grafton, S. T., and Bassett, D. S. (2018). Predicting future learning from baseline network architecture. *Neuroimage*, 172:107–117.

Miller, E. K. and Cohen, J. D. (2001). An integrative theory of prefrontal cortex function. *Annual review of neuroscience*, 24(1):167–202.

Mohr, H., Wolfensteller, U., Betzel, R. F., Mišić, B., Sporns, O., Richiardi, J., and Ruge, H. (2016). Integration and segregation of large-scale brain networks during short-term task automatization. *Nature communications*, 7:13217.

Mucha, P. J., Richardson, T., Macon, K., Porter, M. A., and Onnela, J.-P. (2010). Community structure in time-dependent, multiscale, and multiplex networks. *science*, 328(5980):876–878.

Newman, M. (2018). *Networks*. Oxford university press.

Newman, M. E. and Girvan, M. (2004). Finding and evaluating community structure in networks. *Physical review E*, 69(2):026113.

Onoda, K. and Yamaguchi, S. (2013). Small-worldness and modularity of the resting-state functional brain network decrease with aging. *Neuroscience letters*, 556:104–108.

Park, H.-J. and Friston, K. (2013). Structural and functional brain networks: from connections to cognition. *Science*, 342(6158):1238411.

Pedersen, M., Zalesky, A., Omidvarnia, A., and Jackson, G. D. (2018). Multilayer network switching rate predicts brain performance. *Proceedings of the National Academy of Sciences*, 115(52):13376–13381.

Power, J. D., Barnes, K. A., Snyder, A. Z., Schlaggar, B. L., and Petersen, S. E. (2012). Spurious but systematic correlations in functional connectivity mri networks arise from subject motion. *Neuroimage*, 59(3):2142–2154.

Power, J. D., Cohen, A. L., Nelson, S. M., Wig, G. S., Barnes, K. A., Church, J. A., Vogel, A. C., Laumann, T. O., Miezin, F. M., Schlaggar, B. L., et al. (2011). Functional network organization of the human brain. *Neuron*, 72(4):665–678.

Power, J. D., Mitra, A., Laumann, T. O., Snyder, A. Z., Schlaggar, B. L., and Petersen, S. E. (2014). Methods to detect, characterize, and remove motion artifact in resting state fmri. *Neuroimage*, 84:320–341.

Raichle, M. E., MacLeod, A. M., Snyder, A. Z., Powers, W. J., Gusnard, D. A., and Shulman, G. L. (2001). A default mode of brain function. *Proceedings of the National Academy of Sciences*, 98(2):676–682.

Raven, J. and Raven's Progressive Matrices, M. H. (1994). Manual for raven's progressive matrices and mill hill vocabulary scales. advanced progressive matrices.

Rubinov, M. and Sporns, O. (2011). Weight-conserving characterization of complex functional brain networks. *Neuroimage*, 56(4):2068–2079.

Schaefer, A., Kong, R., Gordon, E. M., Laumann, T. O., Zuo, X.-N., Holmes, A. J., Eickhoff, S. B., and Yeo, B. T. (2017). Local-global parcellation of the human cerebral cortex from intrinsic functional connectivity mri. *Cerebral Cortex*, pages 1–20.

Shine, J. M., Bissett, P. G., Bell, P. T., Koyejo, O., Balsters, J. H., Gorgolewski, K. J., Moodie, C. A., and Poldrack, R. A. (2016). The dynamics of functional brain networks: integrated network states during cognitive task performance. *Neuron*, 92(2):544–554.

Shine, J. M. and Poldrack, R. A. (2018). Principles of dynamic network reconfiguration across diverse brain states. *NeuroImage*, 180:396–405.

Shulman, G. L., Fiez, J. A., Corbetta, M., Buckner, R. L., Miezin, F. M., Raichle, M. E., and Petersen, S. E. (1997). Common blood flow changes across visual tasks: Ii. decreases in cerebral cortex. *Journal of cognitive neuroscience*, 9(5):648–663.

Siegel, J. S., Seitzman, B. A., Ramsey, L. E., Ortega, M., Gordon, E. M., Dosenbach, N. U., Petersen, S. E., Shulman, G. L., and Corbetta, M. (2018). Reemergence of modular brain networks in stroke recovery. *Cortex*, 101:44–59.

Simon, H. A. (1962). The architecture of complexity. In *Facets of systems science*, pages 457–476. Springer.

Snijders, T. and Bosker, R. (2012). Discrete dependent variables. *Multilevel analysis: an introduction to basic and advanced multilevel modeling*, pages 304–307.

Song, J., Birn, R. M., Boly, M., Meier, T. B., Nair, V. A., Meyerand, M. E., and Prabhakaran, V. (2014). Age-related reorganizational changes in modularity and functional connectivity of human brain networks. *Brain connectivity*, 4(9):662–676.

Sporns, O. (2013). Network attributes for segregation and integration in the human brain. *Current opinion in neurobiology*, 23(2):162–171.

Spreng, R. N., Stevens, W. D., Chamberlain, J. P., Gilmore, A. W., and Schacter, D. L. (2010). Default network activity, coupled with the frontoparietal control network, supports goal-directed cognition. *Neuroimage*, 53(1):303–317.

Tononi, G., Sporns, O., and Edelman, G. M. (1994). A measure for brain complexity: relating functional segregation and integration in the nervous system. *Proceedings of the National Academy of Sciences*, 91(11):5033–5037.

Tustison, N. J., Avants, B. B., Cook, P. A., Zheng, Y., Egan, A., Yushkevich, P. A., and Gee, J. C. (2010). N4itk: improved n3 bias correction. *IEEE transactions on medical imaging*, 29(6):1310–1320.

Vatansever, D., Menon, D. K., Manktelow, A. E., Sahakian, B. J., and Stamatakis, E. A. (2015). Default mode dynamics for global functional integration. *Journal of Neuroscience*, 35(46):15254–15262.

Vatansever, D., Menon, D. K., and Stamatakis, E. A. (2017). Default mode contributions to automated information processing. *Proceedings of the National Academy of Sciences*, 114(48):12821–12826.

Vincent, J. L., Kahn, I., Snyder, A. Z., Raichle, M. E., and Buckner, R. L. (2008). Evidence for a frontoparietal control system revealed by intrinsic functional connectivity. *Journal of neurophysiology*, 100(6):3328–3342.

Whitfield-Gabrieli, S. and Nieto-Castanon, A. (2012). Conn: a functional connectivity toolbox for correlated and anticorrelated brain networks. *Brain connectivity*, 2(3):125–141.

Zhang, Y., Brady, M., and Smith, S. (2001). Segmentation of brain mr images through a hidden markov random field model and the expectation-maximization algorithm. *IEEE transactions on medical imaging*, 20(1):45–57.

SUPPLEMENTARY INFORMATION

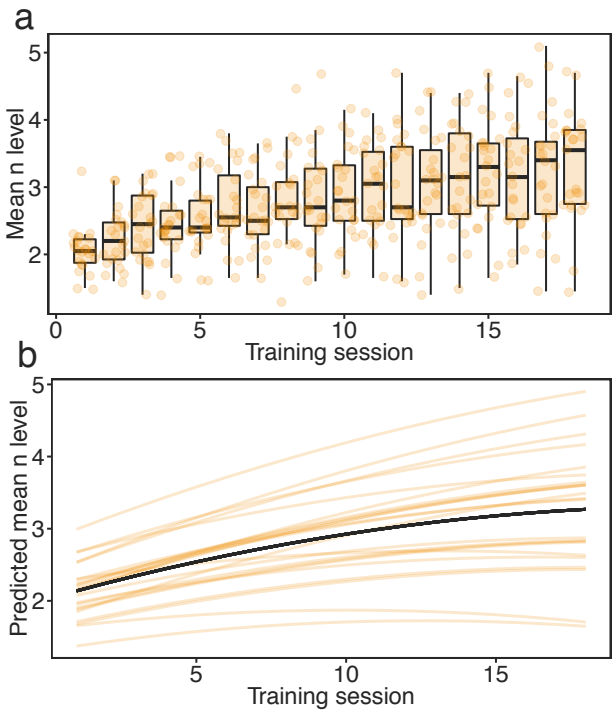

Figure S1: **Behavioral performance during dual n-back training.** The performance was measured as a mean n-back level achieved during each trial of 18 training sessions. This measure was estimated only for the experimental group. (a) Boxplots represent values of mean n-level achieved during 18 sessions of training. Error bars represent 95% confidence intervals. On average, participants improved their initial performance by 60.3%. Maximum n-back levels achieved by participants varied from 3-back to 7-back. (b) Growth model fitted to mean n-values. We fitted both linear and quadratic models to predict the behavioral score (mean n-back level) monitored across the 18 training sessions. Training session significantly predicted mean n-back level achieved by participants, $\chi^2(2) = 111.21$, $p < 0.0001$. Including a quadratic term in the model based on session significantly improved the model fit, $\chi^2(1) = 24.12$, $p < 0.0001$. Orange lines represent models of behavioral improvement fitted to each participant's performance. The black line represents the prototype model fitted to the experimental group. See Figure S2 for individual values of behavioral performance measures.

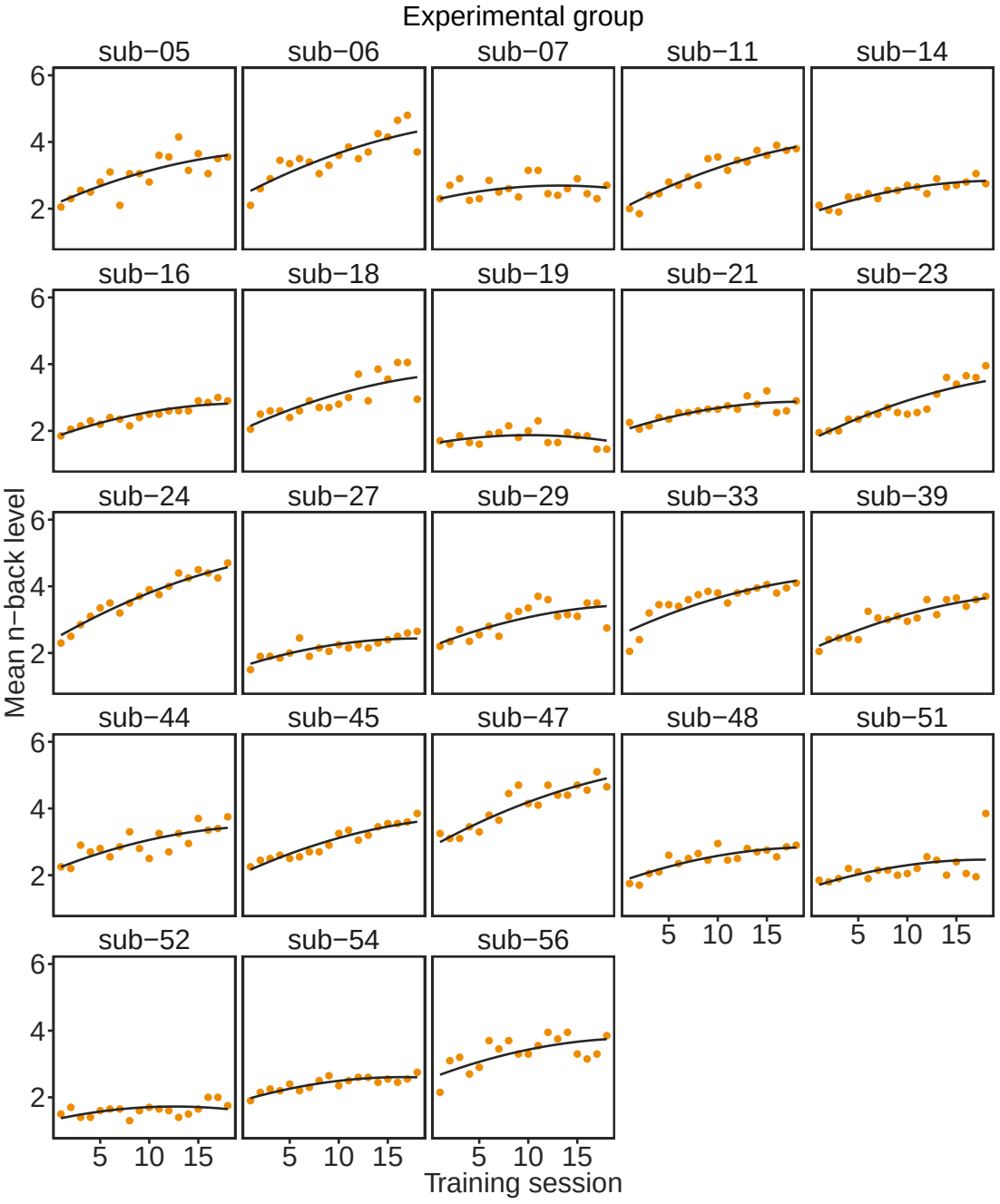

Figure S2: **Individual values of mean n-back level achieved in each session of the dual n-back training.** The black line represents a quadratic model fitted to individual data.

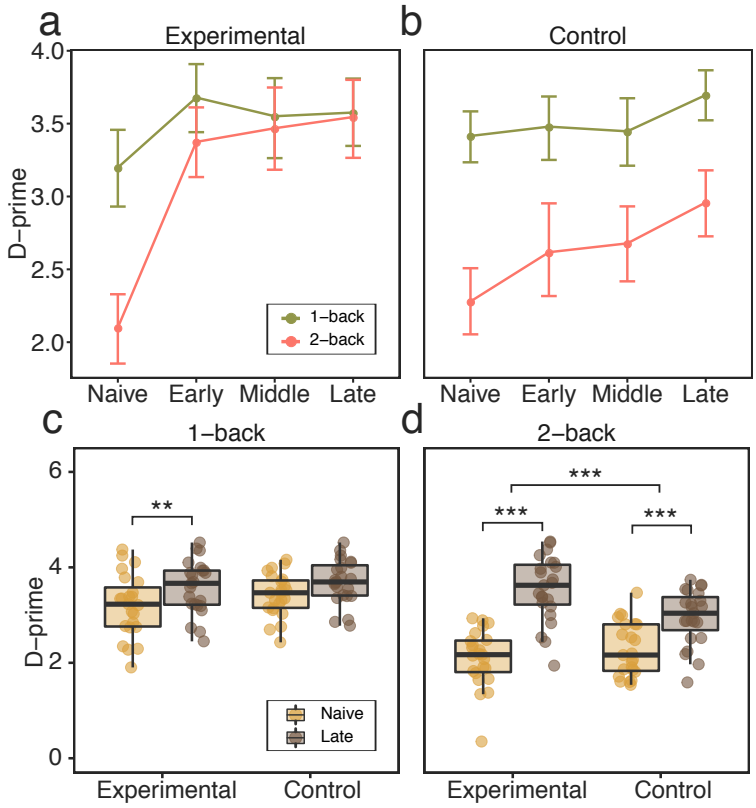

Figure S3: **Behavioral performance modulated by training**. (a, b) Line plots represent mean behavioral performance measured as d-prime, calculated for all training phases (Naive, Early, Middle, Late), dual n-back conditions (1-back and 2-back), and groups (experimental, (a); control, (b)). Participants exhibited significantly different d-prime, depending on the training stage (Naive, Early, Middle, Late), condition (1-back versus 2-back), and group (experimental versus control), as indicated by a χ^2-test ($\chi^2(3) = 9.97$, $p = 0.019$). Error bars represent 95% confidence intervals. (c) The experimental group exhibited an increase in d-prime of 11.8% when comparing the 'Naive' and 'Late' training phases, as measured during the 1-back condition (Bonferroni-corrected, $t(22) = -2.78$, $p = 0.011$); no improvement was found in the control group ($t(22) = -2.29$, $p = 0.032$, not significant after Bonferroni correction). The change in d-prime during the 1-back condition was also not different between the two groups ($t(43.56) = -0.52$, $p = 0.60$). (d) The largest increase in d-prime (68.8%) was observed in the experimental group when comparing 'Naive' and 'Late' training phases, as measured during the 2-back condition (Bonferroni-corrected, $t(22) = -9.08$, $p < 0.0001$). For comparison, the control group exhibited a 29.8% increase in d-prime during the 2-back condition (Bonferroni-corrected, $t(22) = -7.25$, $p < 0.0001$). The change in d-prime was significantly larger for the experimental group than for the control group (Bonferroni-corrected, $t(35.63) = -4.14$, $p = 0.0002$). After training, the experimental group exhibited no difference in behavioral performance between the 1-back and 2-back conditions (Bonferroni-corrected, $t(22) = 0.37$, $p = 0.71$). *** $p < 0.001$ Bonferroni corrected; ** $p < 0.01$ Bonferroni corrected, * $p < 0.05$ uncorrected.

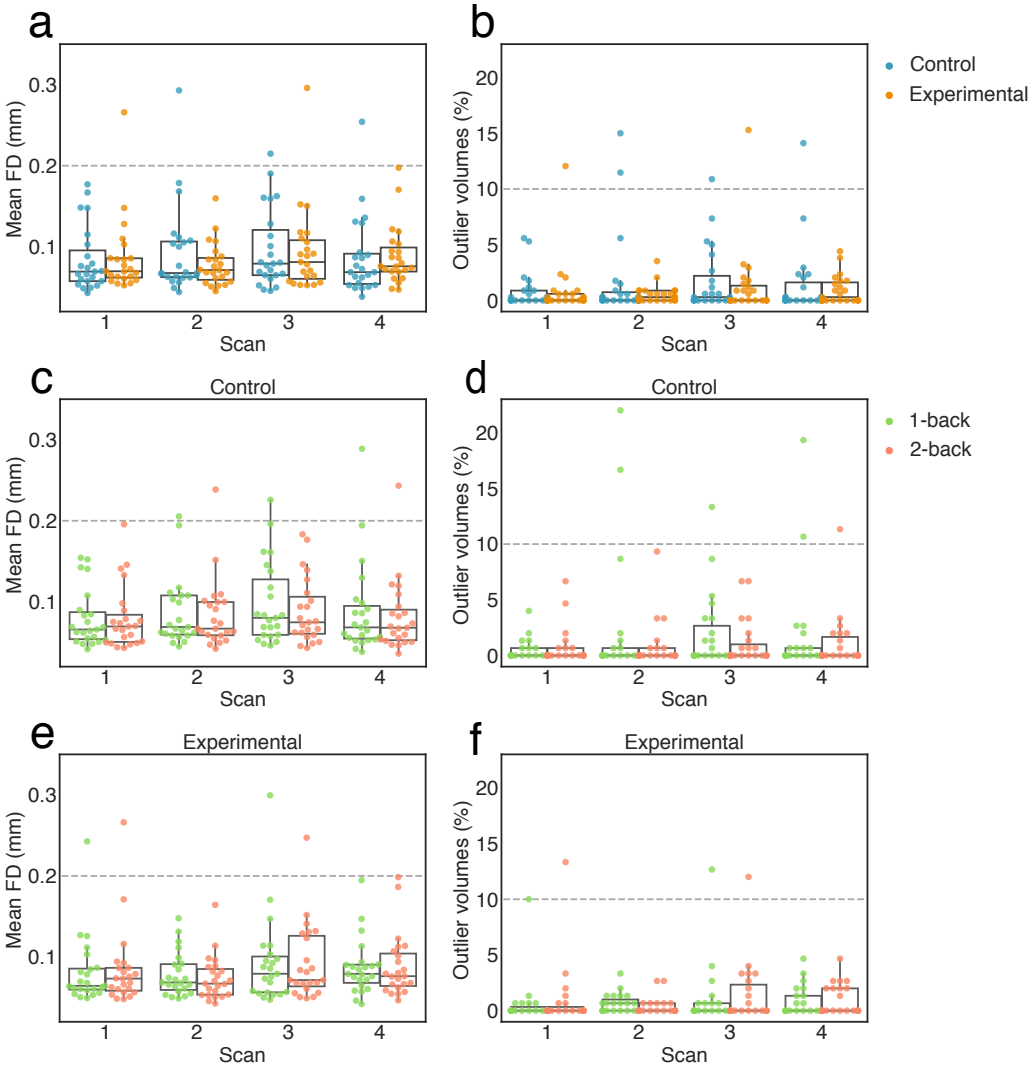

Figure S4: **Head motion during the dual n-back task**. In addition to including 24 motion parameters in the denoising procedure, we also excluded high motion subjects from subsequent analyses. We defined a high motion subject as one with mean frame displacement (FD) larger than 0.2 mm and more than 10% of outlier volumes detected during scrubbing in any scanning session. This criterion was applied when considering the total time courses, as well as when considering time courses of the 1-back and 2-back conditions, separately. As a result we excluded four participants (2 from the control group, and 2 from the experimental group). One subject displayed excessive motion during three scanning sessions, while another displayed excessive motion during two scanning sessions, and two subjects displayed excessive motion in only one scanning session. After excluding high motion subjects, we compared the mean FD and mean percent of outlier scans between sessions, groups, and conditions (see S1 for further details). We did not find significant differences between any of these variables between sessions (all $p < 0.05$), groups (all < 0.05), and most of the condition comparisons. The only difference that passed an uncorrected threshold of significance ($p < 0.05$) was found between the 1-back and 2-back conditions of the control group during the third scanning session.

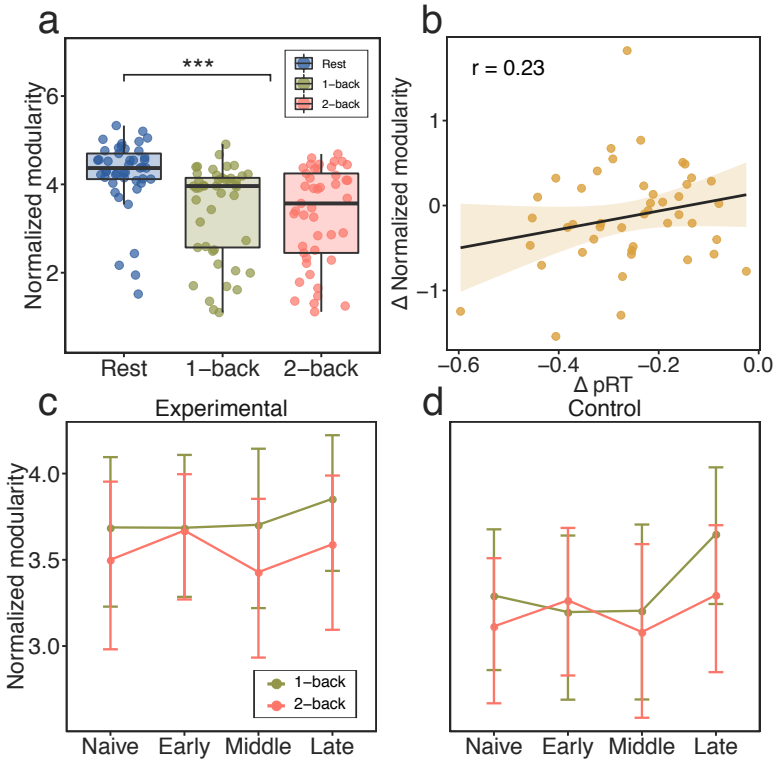

Figure S5: **Whole-brain modularity obtained for the Schaefer parcellation.** (a) Modularity differences between the resting state and the dual n-back task, as well as between the 1-back task condition and the 2-back task condition. (b) Pearson's correlation coefficient between the change (2-back minus 1-back) of normalized modularity and the change (2-back minus 1-back) of behavioral performance measured as penalized reaction time (pRT) (not significant, $p < 0.13$). (c, d) Line plots representing mean values of modularity for each scanning session (Naive, Late, Middle, Late) and condition, separately for the experimental group (c) and for the control group (d).

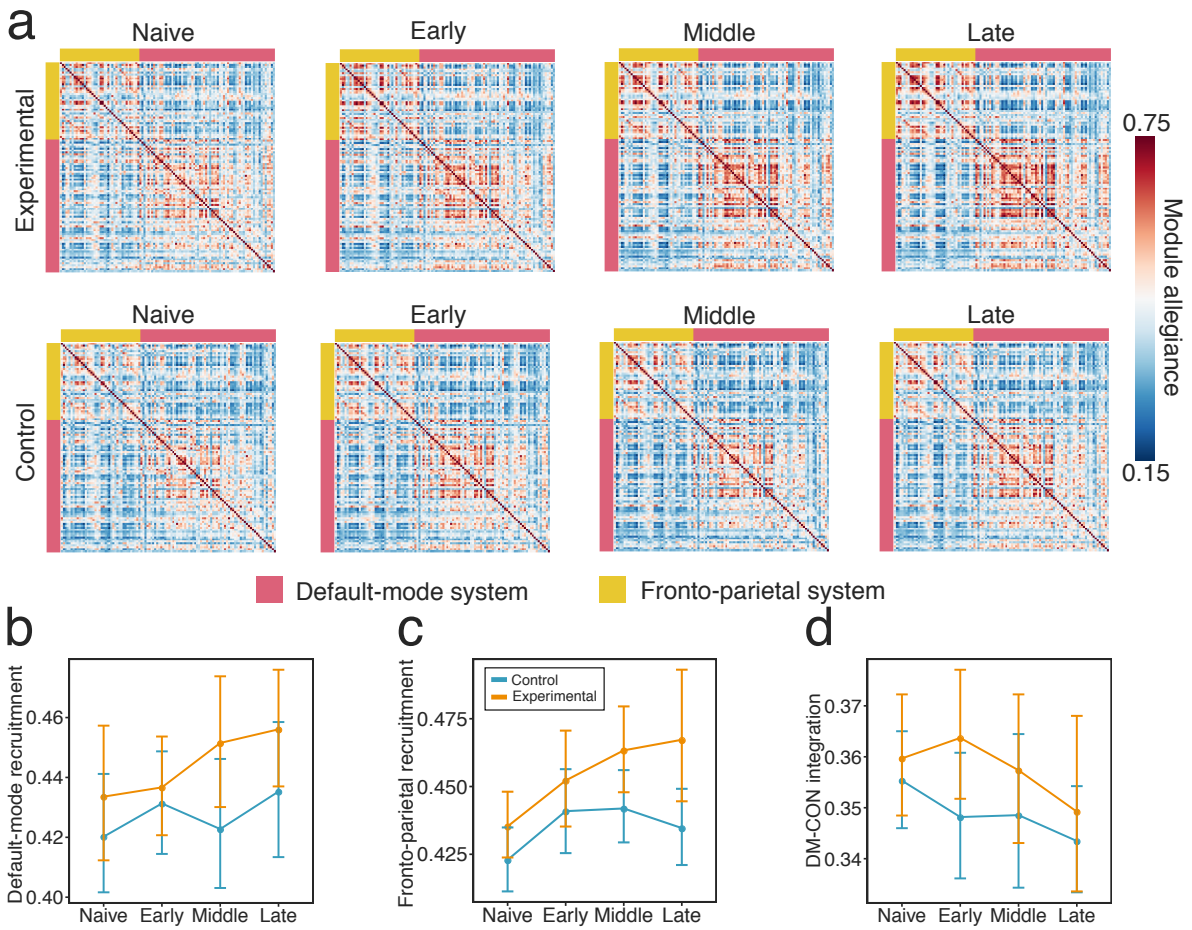

Figure S6: **Training-related changes in module allegiance for the subgraph of the network composed of the default mode and fronto-parietal control (CON) systems calculated using the Schaefer parcellation.** Module allegiance matrices of the default mode system and the fronto-parietal control system (CON). Each ij-th element of the module allegiance matrix represents the probability that node i and node j are assigned to the same community within a single layer of the multilayer network representing task conditions pooled across all scanning sessions. (b) Mean default mode system recruitment across sessions. (c) Mean CON recruitment across sessions. (d) Mean integration between the default mode and CON systems across sessions. Only CON recruitment exhibited a significant main effect of session ($p < 0.002$).

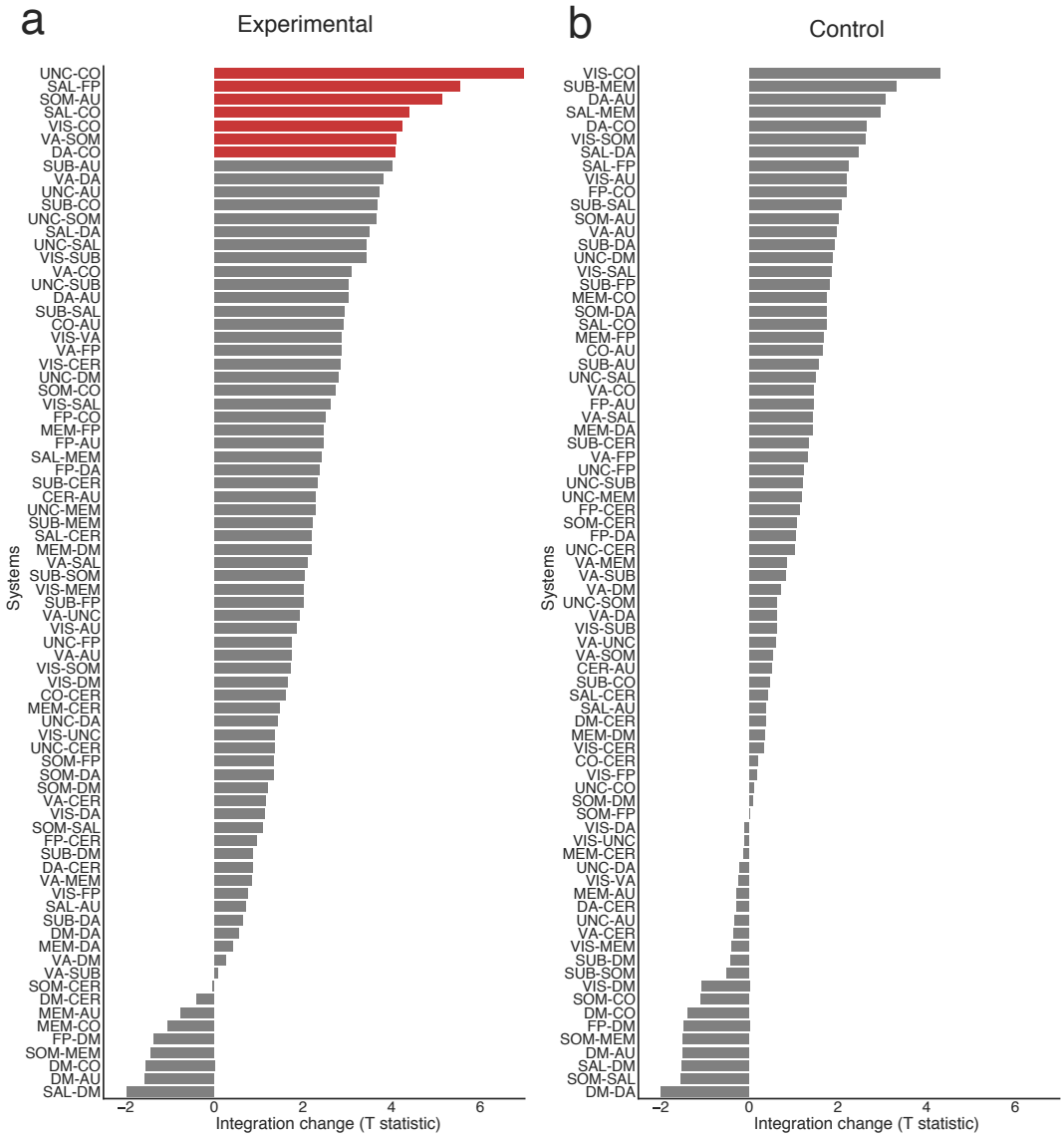

Figure S7: **The training-induced change in integration from the 'Naive' to 'Late' stages between 13 large-scale systems defined in the Power parcellation.** Left panel (**a**) shows integration change of the experimental group. Right panel (**b**) shows integration change of the control group. Red boxes represent a significant change in integration after Bonferroni correction.

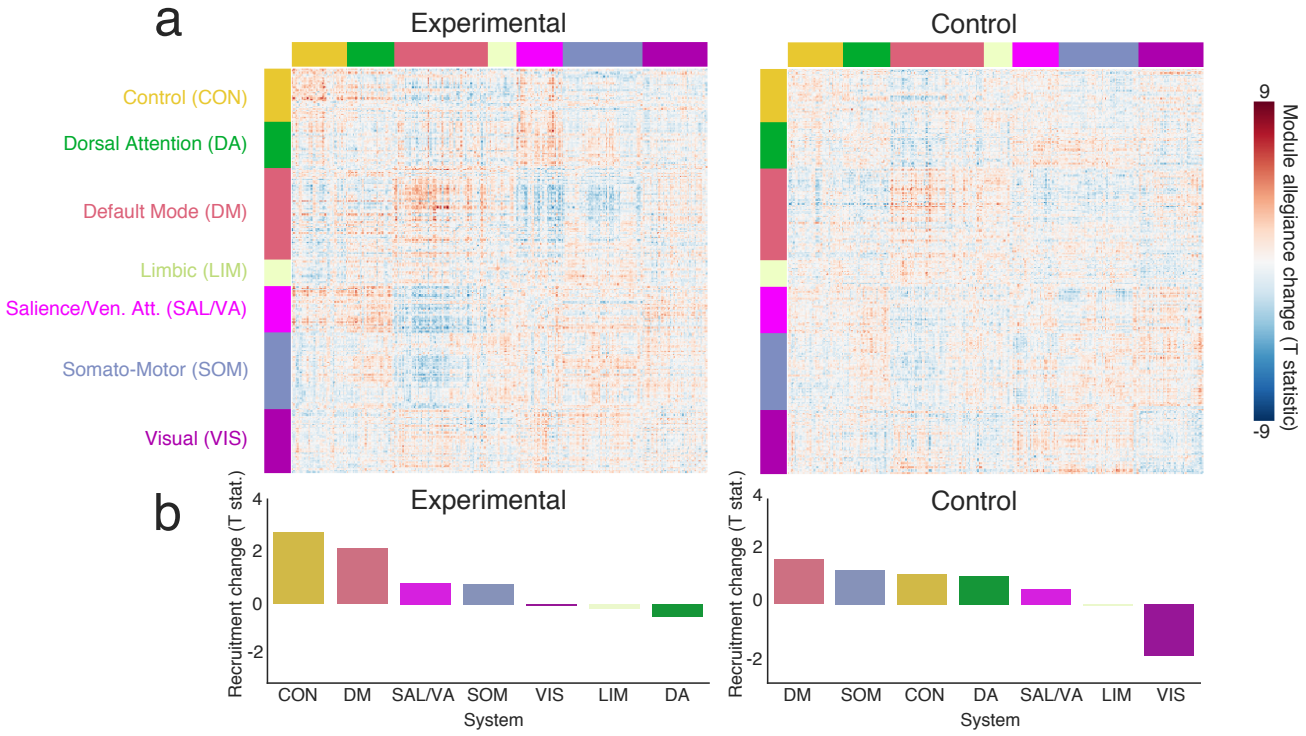

Figure S8: **Whole-brain changes in module allegiance between the 'Naive' and 'Late' stages for the Schaefer parcellation (7 systems).** (**a**) Changes in node allegiance as reflected in t-statistic values from a two-tailed t-test. (**b**) The largest mean recruitment changes were observed for the default mode (DM) and fronto-parietal (FP) systems.

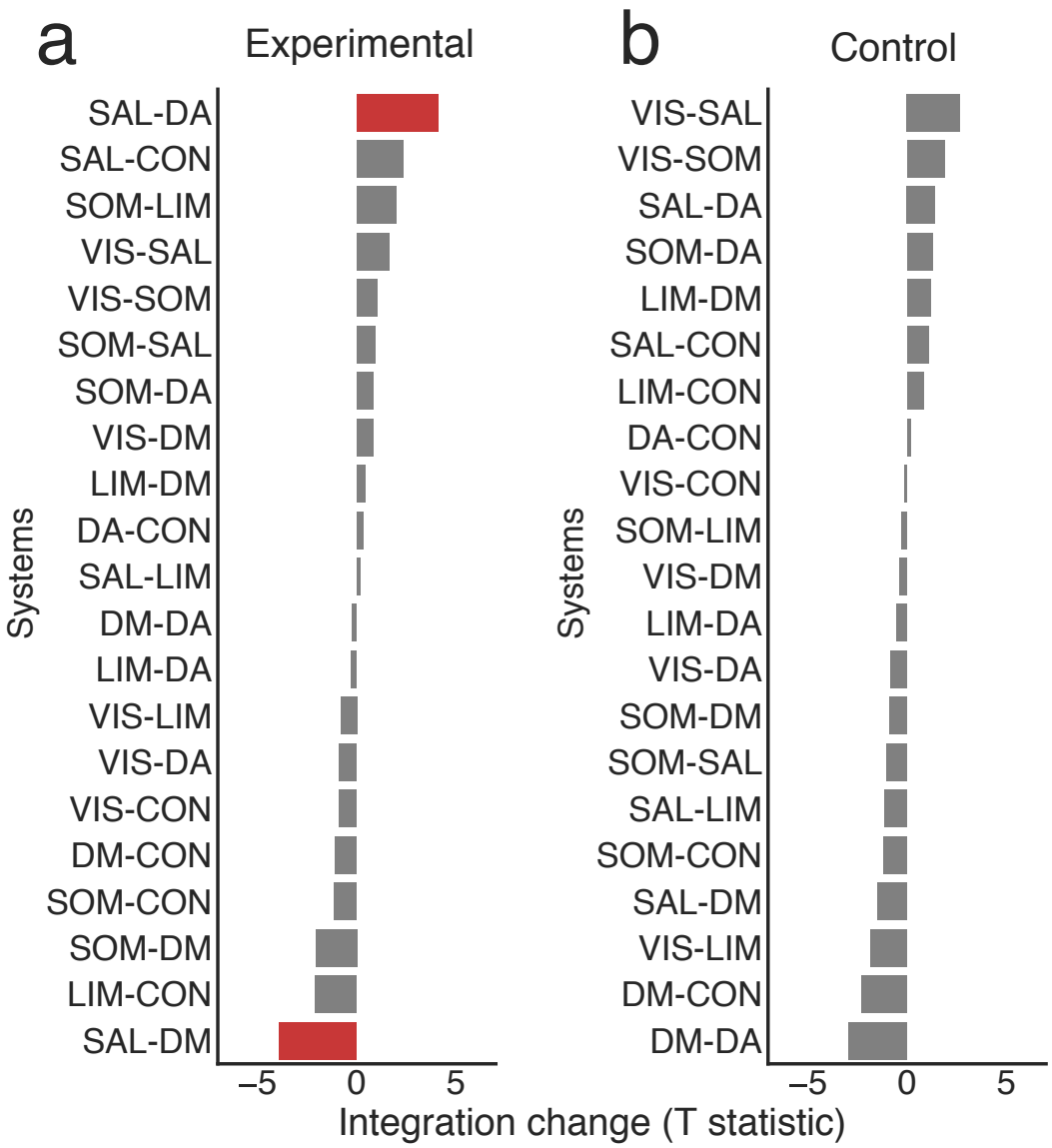

Figure S9: **The training-induced change in integration from the 'Naive' to 'Late' between 7 large-scale systems of the Schaefer parcellation.** Left panel (**a**) shows the change in integration change for the experimental group. Right panel (**b**) shows the change in integration for the control group. Red boxes represent a significant change in integration after Bonferroni correction for multiple comparisons.

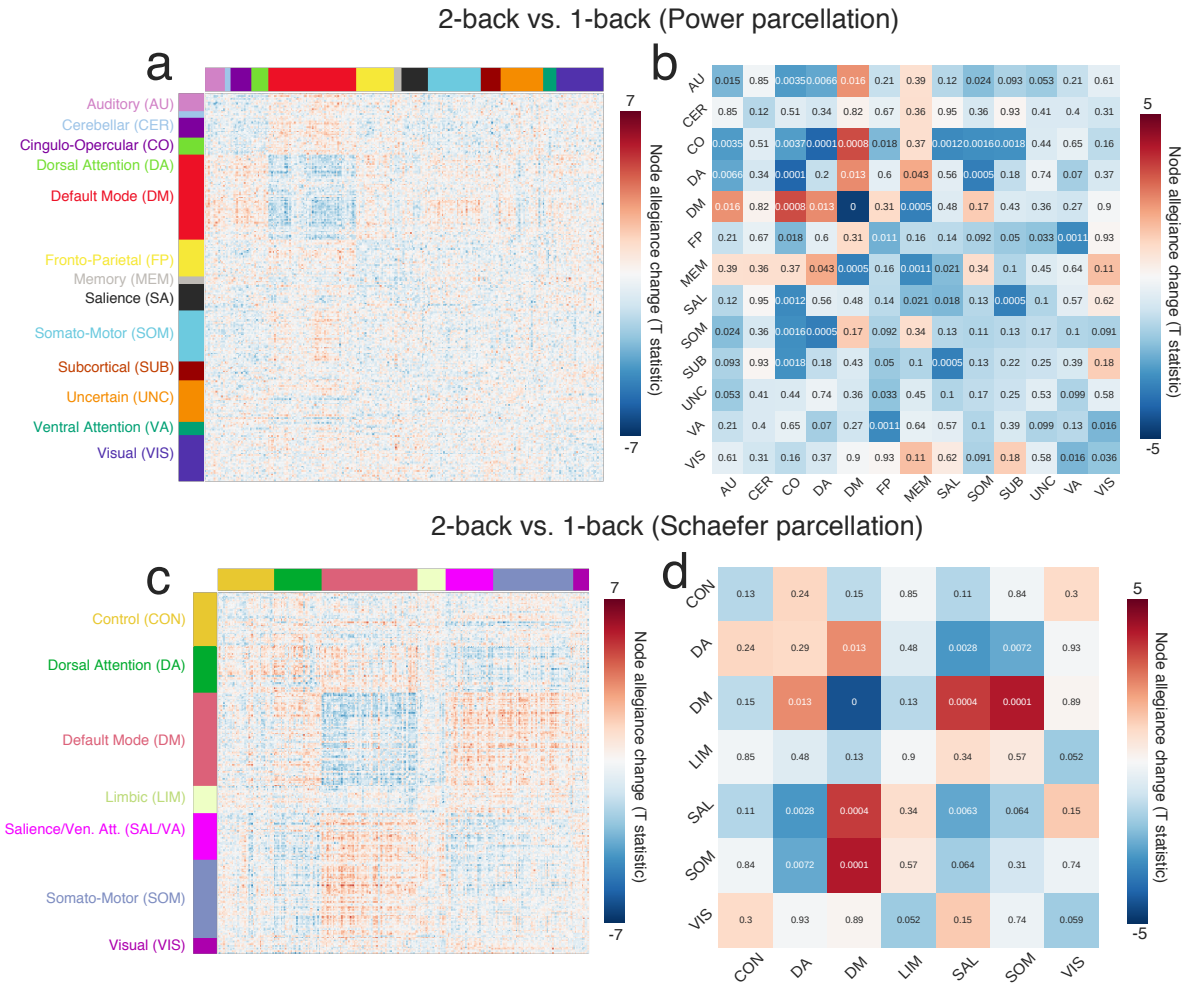

Figure S10: **Differences in module allegiance between the 2-back condition and the 1-back condition for the baseline ('Naive') scanning session**. Top panel: Differences in module allegiance between the 2-back condition and the 1-back condition, calculated for the Power parcellation (264 ROIs). (a) Nodes' change in module allegiance as measured with a paired t-test. (b) Changes in recruitment and integration calculated as the mean allegiance change within and between 13 main large-scale systems. Bottom panel: Differences in the module allegiance between the 2-back condition and the 1-back condition calculated for the Schaeffer (300 ROIs) parcellation. (c) Nodes' change in module allegiance measured with a paired t-test. (d) Change in recruitment and integration calculated as the mean allegiance change within and between 7 large-scale systems.